



Non-Genomic AhR-Signaling Modulates the Immune Response in Endotoxin-Activated Macrophages After Activation by the Environmental Stressor BaP

Henning Großkopf¹, Katharina Walter¹, Isabel Karkossa¹, Martin von Bergen^{1,2} and Kristin Schubert^{1*}

¹ Department of Molecular Systems Biology, Helmholtz Centre for Environmental Research, Leipzig, Germany, ² Institute of Biochemistry, Leipzig University, Leipzig, Germany

OPEN ACCESS

Edited by:

Amiram Ariel,
University of Haifa, Israel

Reviewed by:

Thomas Haarmann-Stemmann,
Leibniz-Institut für
Umweltmedizinische Forschung (IUF),
Germany

Angel L. Corbi,
Consejo Superior de Investigaciones
Científicas (CSIC), Spain

*Correspondence:

Kristin Schubert
kristin.schubert@ufz.de

Specialty section:

This article was submitted to
Inflammation,
a section of the journal
Frontiers in Immunology

Received: 23 October 2020

Accepted: 15 March 2021

Published: 31 March 2021

Citation:

Großkopf H, Walter K,
Karkossa I, von Bergen M and
Schubert K (2021) Non-Genomic AhR-
Signaling Modulates the Immune
Response in Endotoxin-Activated
Macrophages After Activation
by the Environmental Stressor BaP.
Front. Immunol. 12:620270.
doi: 10.3389/fimmu.2021.620270

Emerging studies revealed that the Aryl hydrocarbon receptor (AhR), a receptor sensing environmental contaminants, is executing an immunomodulatory function. However, it is an open question to which extent this is achieved by its role as a transcription factor or *via* non-genomic signaling. We utilized a multi-post-translational modification-omics approach to examine non-genomic AhR-signaling after activation with endogenous (FICZ) or exogenous (BaP) ligand in endotoxin-activated (LPS) monocyte-derived macrophages. While AhR activation affected abundances of few proteins, regulation of ubiquitination and phosphorylation were highly pronounced. Although the number and strength of effects depended on the applied AhR-ligand, both ligands increased ubiquitination of Rac1, which participates in PI3K/AKT-pathway-dependent macrophage activation, resulting in a pro-inflammatory phenotype. In contrast, co-treatment with ligand and LPS revealed a decreased AKT activity mediating an anti-inflammatory effect. Thus, our data show an immunomodulatory effect of AhR activation through a Rac1 ubiquitination-dependent mechanism that attenuated AKT-signaling, resulting in a mitigated inflammatory response.

Keywords: aryl hydrocarbon receptor, macrophages, proteome, ubiquitin, phosphorylation, immunomodulation, Rac1, AKT

INTRODUCTION

The Aryl hydrocarbon receptor (AhR), initially described as an environmental sensor (1), has been shown to play a pivotal role in the modulation of immune cell function (2). Most immune cells, including macrophages, and their progenitors, express the AhR (3–5). On the one hand, AhR can inhibit the differentiation of monocyte-derived and bone marrow-derived macrophages (6, 7). On the other hand, AhR decreases the production of proinflammatory cytokines and increases the secretion of anti-inflammatory IL-10 after pattern recognition receptor (PRR) activation by differentiated macrophages (8). Macrophages of AhR-knockout (Ahr^{-/-}) mice produce higher

amounts of proinflammatory cytokines (TNF- α , IL-6, IL-12). These AhR^{-/-} mice are more sensitive to LPS induced septic shock (9, 10), suggesting an anti-inflammatory effect protecting against immunopathologies (11). However, the underlying molecular mechanisms are not entirely understood.

The AhR is a ligand-activated transcription factor and was first described as a receptor for 2,3,7,8-tetrachlorodibenzo-p-dioxin (TCDD) (1). Additional exogenous chemicals like benzo(a)pyrene (BaP) but also endogenous ligands like the light-dependent Tryptophan metabolite 6-formylindolo[3,2-b]carbazole (FICZ) and metabolites produced by the intestinal microbiota have been shown to activate the AhR (12, 13). AhR is part of a cytosolic complex in its inactive form from which AhR is released upon ligand binding, resulting in AhR translocation to the nucleus (14–17). After dimerization with the aryl hydrocarbon receptor nuclear translocator (ARNT), gene expression from xenobiotic response elements (XRE) is initiated (18). Among the target genes are phase I xenobiotic-metabolizing enzymes, e.g., CYP1A1, CYP1B1, IDO1, and TDO2, as well as the aryl hydrocarbon receptor repressor (AHRR), providing a negative feedback loop (19).

Besides its function as a transcription factor, AhR has been shown to exhibit non-genomic signaling pathways by regulating protein ubiquitination and phosphorylation. The AhR itself can act ligand-dependently as the substrate recognition unit of a cullin 4B ubiquitin ligase complex targeting the estrogen receptor α (ER α) for proteasomal degradation (20). Thereby, the control of AhR localization is a regulatory mechanism to modulate transcriptional activity and ubiquitin ligase function (21). On the other hand, AhR ligand binding can release the tyrosine-protein kinase SRC from the cytosolic AhR-complex in an active form (14), resulting in phosphorylation of the E3 ubiquitin ligase c-CBL and subsequent ubiquitination and degradation of the spleen tyrosine kinase (SYK) in pre-osteoclast after AhR activation with tetrandrine (22).

Both genomic and non-genomic signaling pathways contribute to the AhR-dependent modulation of macrophage activation. Two of the NF- κ B subunits (RelA and RelB) can physically interact with AhR (23, 24). AhR activation by TCDD induces degradation of RelA by the ubiquitin-proteasome pathway. This effect is dependent on AhR transcriptional activity (25). Zhu et al. could demonstrate that non-genomic AhR-signaling participates in immunomodulation through SRC-dependent STAT3 phosphorylation and subsequent anti-inflammatory IL-10 production (26), revealing its importance in immune function. However, although knowledge on non-genomic AhR-signaling is emerging, little is known on the underlying molecular mechanisms in macrophages.

Thus, we aimed to unravel the immunomodulatory properties and the relevant non-genomic signaling events after AhR activation by BaP or FICZ using a multi-PTM-omics approach in endotoxin-stimulated human monocyte-derived macrophages. We analyzed alterations of protein ubiquitination and phosphorylation to elucidate affected signaling pathways after AhR activation and integrated the data to characterize the contribution of non-genomic AhR-signaling in macrophages.

MATERIAL AND METHODS

Cell Culture

Buffy coats were obtained from healthy donors from the Institute of Transfusion Medicine, Leipzig, Germany as approved by the local ethic committee. Peripheral blood mononuclear cells (PBMC) were enriched from buffy coats by Ficoll gradient centrifugation. Primary monocytes were enriched from PBMC by adherence to the surface of cell culture plates for 2h in RPMI 1640 (Life Technologies, USA) supplemented with 5% heat-inactivated FBS (Biowest, France) and Penicillin/Streptomycin (Sigma-Aldrich, USA). Monocytes were collected and differentiated to macrophages by adding 100ng/ml recombinant human M-CSF (PeproTech, Germany) for 5d, as described previously (27). Differentiated macrophages were collected and distributed to new cell culture plates and rested for 24h. Rested macrophages were stimulated with 2 μ M BaP (Sigma-Aldrich, USA), 100nM FICZ (Enzo Biochem, USA), or the same volume DMSO (Sigma-Aldrich, USA) for 2h. All stimulations were additionally conducted with 100ng/ml LPS (InvivoGen, USA). Cells were treated with 2 μ M Perifosine (Cell Signaling Technologies, USA) or 25 μ M RAC1-Inhibitor NSC23766 (ENZ-CHM116, Enzo Life Sciences, USA) 30min before stimulation with AhR-ligands and/or LPS for inhibitor assays. All cell culturing incubations were conducted in a humidified cell incubator at 37°C with 5% CO₂. The cells were lysed with urea lysis buffer (9M urea (Merck, Germany) in 20mM HEPES pH 8.0 (Sigma-Aldrich, USA) supplemented with 1mM sodium orthovanadate (Sigma-Aldrich, USA), 2.5mM sodium pyrophosphate (Sigma-Aldrich, USA), and 1mM b-glycerol-phosphate (Alfa Aesar, USA)) for proteome, ubiquitome, and phosphoproteome analysis. Cell lysis for western blot analysis was conducted with Triton X-100 lysis buffer (1% Triton-X-100 (SERVA, Germany), 150mM NaCl (Roth, Germany), 0.5% Na-deoxycholate (Sigma, USA), 0.5% SDS (SERVA, Germany) in 50mM TrisHCl pH 7.4 (Merck, Germany)).

Fractionation and Digestion for LC-MS/MS-Based Proteomics

The protein concentrations of the samples were determined utilizing the Pierce 660 nm proteins assay (Thermo Fisher, USA). For global proteome analysis, 30 μ g protein were pre-fractionated by SDS-PAGE as previously described (28). Each sample lane was cut in 5 slices with approximately the same protein amount after Coomassie staining. All fractions were reduced with 100 mM DTT (Merck, Germany), carbamidomethylated with 100 mM IAA (Merck, Germany), and proteolytically cleaved in-gel utilizing Trypsin (Roche, Switzerland) applied in a 1:40 Trypsin/protein ratio. The resulting peptides were extracted with 50% ACN in 0.01% FA. Peptide extracts were evaporated with a vacuum-concentrator and reconstituted in 0.1% FA for LC-MS/MS measurement. Seven biological replicates (n = 7) were used for proteome analysis.

Ubiquitin-Remnant-Motif (K-E-GG) Analysis

Ubiquitome analysis was conducted by PTMScan[®] Discovery Proteomic Services (Cell Signaling Technology, Danvers, MA,

USA). In short, pooled lysates from nine donors were digested using Trypsin, and peptides with the ubiquitin-remnant-motif (K- ϵ -GG-remnant), which is left on ubiquitinated lysine residues after tryptic digestion, were enriched utilizing a proprietary antibody. All Ub-remnant enriched samples were measured in technical duplicates by LC-MS/MS.

Phosphopeptide Enrichment

For phosphopeptide enrichment, samples were proteolytically cleaved using a paramagnetic bead approach (29, 30). In short, 600 μ g protein of each sample was precipitated on Magnetic Carboxylate Modified Particles (Sigma-Aldrich, USA), reduced with 50 mM TCEP (Sigma-Aldrich, USA), carbamidomethylated with 100 mM IAA (Merck, Germany), and proteolytically cleaved with Trypsin (Promega, USA) applied in a 1:50 Trypsin/protein ratio. Peptides were collected and dried to completeness using a vacuum concentrator.

Phosphopeptides were sequentially enriched by TiO₂- and Fe-NTA-based affinity chromatography. Firstly, the High-Select™ TiO₂ Phosphopeptide Enrichment Kit (Thermo Scientific, USA) was used following the manufacturer's instructions. Flow-through of peptide samples and first wash fractions were combined and dried to completeness for the following second enrichment step. Secondly, the High-Select™ Fe-NTA Phosphopeptide Enrichment Kit (Thermo Scientific, USA) was used following the manufacturer's instructions. Phosphopeptide enriched eluates from both steps were combined, dried to completeness, and reconstituted in 0.1 % FA for LC-MS/MS measurement. Four biological replicates (n = 4) were conducted for Phosphopeptide enrichment.

LS-MS/MS

LC-MS/MS analysis of samples was performed on an UltiMate 3000 RSLCnano system (Dionex, USA), online coupled to a Q Exactive HF mass spectrometer (Thermo Fisher Scientific, USA) by a chip-based electrospray ionization source (TriVersa NanoMate, Advion, USA). Peptides were trapped and desalinated on a C18 pre-column (Acclaim PepMap 100, 75 μ m x 2 cm, C18, 3 μ m), and subsequently separated on a C18 analytical column (Acclaim PepMap RSLC, 75 μ m x 25 cm, C18, 2 μ m).

For proteome analysis, a previously described bipartite linear 55 min gradient starting from 4 % eluent B (0.1 % FA in 80 % ACN) in eluent A (0.1 % FA in water) to 55 % eluent B *via* 30 % eluent B after 47.5 min was used (28). After each sample, the column was flushed to 99% eluent B and reconstituted to starting conditions. Mass spectra were acquired in a data-dependent manner. For MS1 scans, the following parameters were set: m/z range 350-1550, maximum injection time = 100 ms, automated gain control (AGC) = 3×10^6 , R = 60 000. The top 10 most abundant ions were selected for MS2 acquisition using the following parameters: isolation window of 1.4 m/z, maximum injection time 100 ms, AGC = 2×10^5 , normalized collision energy (NCE) = 28, R = 15 000, m/z range 200-2000. Fragmented ions were dynamically excluded for 20 s.

For phosphopeptide analysis, a tripartite linear 145 min gradient starting from 4 % eluent B (0.1 % FA in 80 % ACN)

in eluent A (0.1 % FA in water) to 55 % eluent B *via* 18 % eluent B after 77.5 min and 30 % eluent B after 115 min was used. After each sample, the column was flushed to 99% eluent B and reconstituted to starting conditions. Mass spectra were acquired in a data-dependent manner. For MS1 scans the following parameters were set: m/z range 350-1550, maximum injection time = 120 ms, AGC = 3×10^6 , R = 120 000. The top 15 most abundant ions were selected for MS2 acquisition using the following parameters: isolation window of 0.7 m/z, maximum injection time 150 ms, AGC = 2×10^5 , normalized collision energy (NCE) = 28, R = 15 000, m/z range 200-2000. Fragmented ions were dynamically excluded for 45 s.

Data Analysis

The LC-MS/MS raw data for proteome and phosphoproteome were examined by MaxQuant (Version 1.6.7.0) (31). Database search was performed against the Uniprot Homo Sapiens RefSet (09/2019, 74349 entries) and a list of common contaminants provided by MaxQuant (07/2019, 245 entries) (32). Search parameters were set as follows: Maximum missed cleavages = 2, minimal peptide length = 6 amino acids, first search peptide tolerance = 20 ppm, main search peptide tolerance = 4.5 ppm, FTMS MS/MS match tolerance = 20 ppm. Carbamidomethylation of cysteine was set as fixed modification, protein N-terminal acetylation, oxidation of methionine, and, for phosphopeptide enriched samples, phosphorylation of Serin, Threonine, and Tyrosine were set as variable modifications. Peptides, proteins, and sites were filtered by a target-decoy approach to an FDR ≤ 0.01 using a reversed decoy database. Match between runs was enabled with a match time window of 0.7 min and alignment time window of 20 min. Label-free quantification (LFQ) was used for relative protein quantification based on an LFQ ratio count ≥ 2 .

Proteins and phosphosites identified by site, from the reverse database, or as potential contaminants were removed. R-3.6.1 was used for further statistical analysis using the following packages: limma (33), plyr (34), reshape2 (35), xlsx (36), DEP (37), ggsci (38), circlize (39), calibrate (40), ggplot2 (41), readxl (42), qpcR (43), splitstackshape (44), tidyr (45), and Tmisc (46). (LFQ-) intensities were log₂-transformed and median normalized. To be considered as reliably quantified, proteins or PP-sites had to be quantified in more than 50% of replicates. Imputation was done for proteins and PP-sites completely not quantified in one condition but reliably quantified in the second condition of the comparison. Significantly altered proteins and PP-sites were then identified by Student's t-test. The test was chosen because of its applicability to the used quantification method, number of biological replicates, and statistical power (47). Using this test, false positives are expected evenly distributed among all quantified proteins and phosphosites, while true changes cluster in relevant altered pathways. Hence, pathway- and enrichment-based analysis provide an additional filter (48). The down-stream analysis was largely based on enrichment analyses for pathways and inference of kinase activities. The threshold for significant alteration was set at $p \leq 0.01$ without FDR correction to evade double filtering but limit the number of by chance false positives.

Functional annotation regarding KEGG and Reactome pathways was done with DAVID bioinformatics resources (49). Ingenuity pathway analysis (IPA) was used for phosphorylation-dependent pathway analysis. Molecules and relationships were restricted the following: species = human, confidence = experimentally observed, tissues = monocyte-derived macrophages. Only pathways with a p -value ≤ 0.01 were used for further analyses. Kinase activities were inferred by integrating amino acid sequence windows of significantly altered PP-sites with kinase-substrate motifs utilizing KinSwingR (50) in the R environment. Kinase substrate motifs were calculated based on the kinase-substrate dataset from PhosphoSitePlus (downloaded 12/2019) (51).

Enzyme-Linked Immunosorbent Assay (ELISA)

Supernatants of monocyte derived macrophages were collected after stimulation and analyzed for TNF, IL1 β and NO release. The BD OptEIA™ Human TNF ELISA Set (BD Biosciences, USA), BD OptEIA™ Human IL1 β ELISA Set (BD Biosciences, USA), and Total Nitric Oxide and Nitrate/Nitrite Parameter Assay Kit (Bio-Techne, Germany) were applied according to the manufacturer's protocol.

Quantification of mRNA Expression Levels

Total RNA was isolated using the RNeasy kit (QIAGEN, Germany), and single stranded cDNA was synthesized using the High Capacity cDNA Reverse Transcription Kit (Thermo Fisher, USA). The qPCR was performed using TaqMan™ Fast Advanced Master Mix (Thermo Fisher, USA) and a qPCR ABI 7500 Fast Real-Time PCR System (Applied Biosystems, USA). The following primers were used 1) Hs00164383_m1, CYP1B1, FAM-MGB 2) Hs00174128_m1, TNFalpha, FAM-MGB 3) Hs00420895_gH, RPLPO, FAM-MGB 4) Hs01005075_m1, AHRR, FAM-MGB 5) Hs01054794_m1, CYP1A1, FAM-MGB (all Thermo Fisher, USA). Fold changes were calculated by the $\Delta\Delta C_t$ -Method relative to the unstimulated control with RPLPO as the reference (52).

Western Blot Analysis

Cell lysates were separated by SDS-PAGE (10%), and transferred onto a nitrocellulose membrane. Membranes were blocked in 3% BSA in TBS-T (0.05% Tween20 in Tris-buffered saline) for 1h, followed by incubation with primary antibody overnight at 5°C. The following primary antibodies were used: β -Actin (#3700, Cell Signaling Technologies, USA), phospho-AKT Ser473 (#9271, Cell Signaling Technologies, USA), AKT (#9272, Cell Signaling Technologies, USA), AhR (sc-133088, Santa Cruz Biotechnology, USA) and CDKN1A (#2947, Cell Signaling Technologies, USA). Immunoblots were washed with TBS-T, and incubated with HRP-coupled secondary anti-rabbit (#1706515, Biorad, USA) or anti-mouse (#7076, Cell Signaling Technologies, USA) antibody for 1h at room temperature. After washing 3-times with TBS-T, chemiluminescence signal was detected using the FluorChem FC3 imager (ProteinSimple,

USA). Quantification was performed using AlphaView SA (Version 3.5.0.927, ProteinSimple, USA).

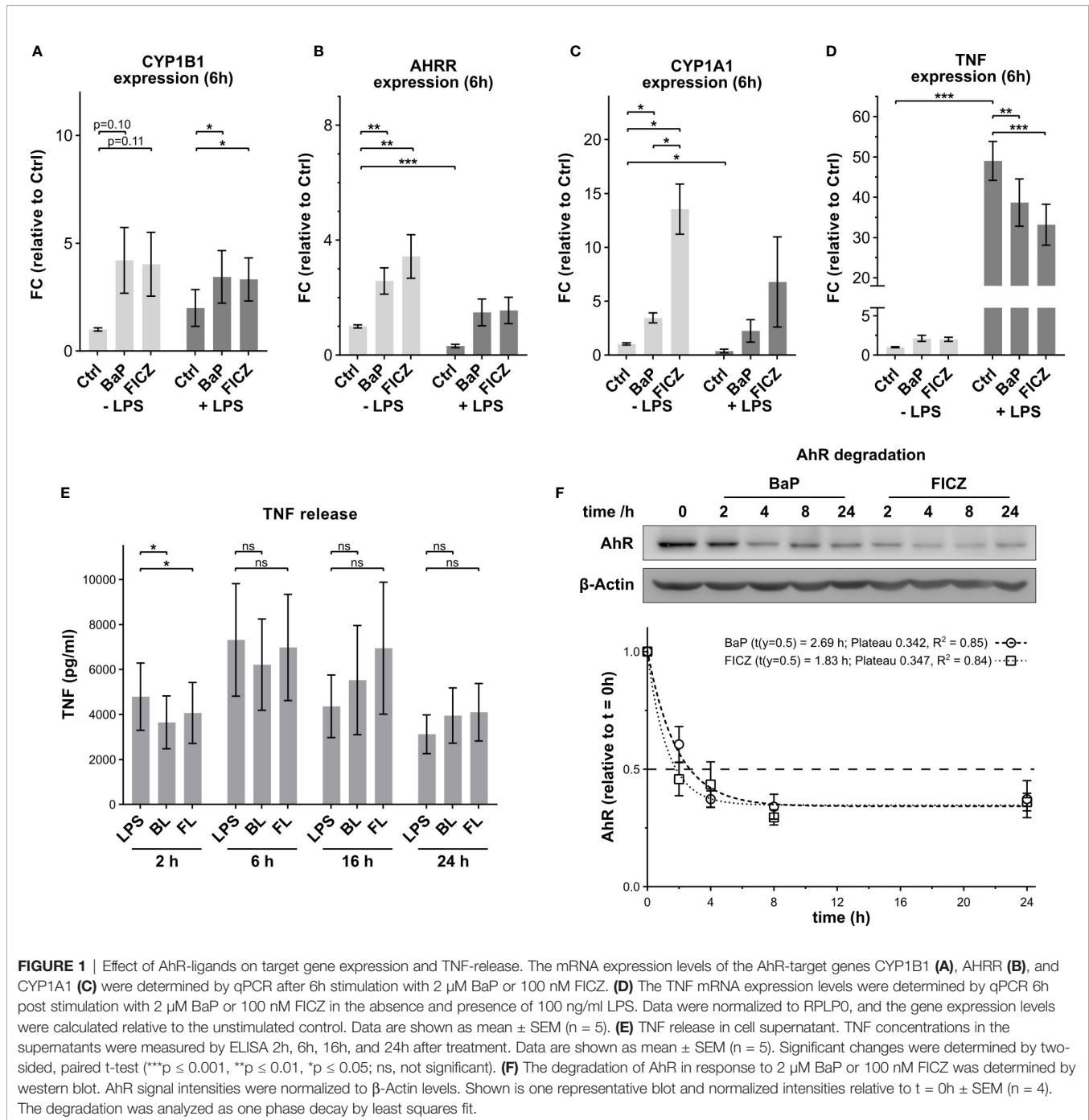
RESULTS

Effect of AhR-Ligands on Target Gene Expression and TNF-Release

To study the immunomodulatory properties of non-genomic AhR-signaling in macrophages, we investigated the effects of an endogenous (FICZ) and an exogenous (BaP) AhR ligand. The effects of BaP and FICZ on AhR-target gene expression were evaluated in human monocyte derived-macrophages to confirm comparable capacities of AhR activation. After 6h of treatment, both ligands led to a ~4-times induction of CYP1B1 mRNA expression (**Figure 1A**) at the used concentrations of 2 μ M (BaP) and 100 nM (FICZ). The AhR repressor (AHRR) was increased 2.8-times by BaP and 3.2-times by FICZ (**Figure 1B**). In contrast, the induction of CYP1A1 expression was about 3-times stronger after FICZ-treatment, than after BaP-treatment. Co-treatment with either of the two ligands and 100 ng/ml LPS attenuated the AhR-ligand dependent induction of AHRR and CYP1A1, but not CYP1B1 (**Figures 1A–C**). The stimulation of macrophages with LPS strongly induced TNF mRNA expression by a factor of ~50. Co-treatment with the AhR-ligands BaP and FICZ inhibited this induction by 21% and 32%, respectively, while AhR activation alone led to a slight increase of TNF-mRNA levels (**Figure 1D**). Thus, BaP and FICZ activated AhR to a comparable extent at the given concentrations, and both ligands had an inhibiting effect on TNF expression after LPS-treatment.

To evaluate the effects of AhR activation, macrophages were treated for 2h, 6h, 16h and 24h with the respective AhR-ligands with and without LPS. After 2h, the AhR activation by BaP or FICZ in combination with LPS, subsequently termed BL and FL, mitigated the LPS-induced TNF-release indicating a modulatory effect (**Figure 1E**). BaP and FICZ reduced the LPS-dependent TNF-release by 23% and 17%, respectively, while the AhR-ligands did not affect the TNF-release without LPS-co-stimulation (**Supplementary Figure 1A**). With longer incubation time, the repression of TNF-release by the AhR-ligands diminished after 6h. Neither LPS-treatment, nor treatment with AhR-ligands alone or in combination with LPS-induced release of nitric oxide after 2h (**Supplementary Figure 1B**). Additionally, co-treatment with LPS and AhR-ligand had no significant effect on the release of IL1 β compared to LPS alone (**Supplementary Figure 1C**). The IL1 β levels in the supernatant were minute after 2h and increased over the complete observation time. Beginning after 16h, AhR-stimulation showed an augmenting effect on the LPS-induced IL1 β release, although this effect was not statistically significant.

Previous reports showed that AhR is rapidly degraded after activation in hepatocytes. Thereby, nuclear export of AhR precedes the degradation by the 26S-proteasome with a half-life of 2–3h (53, 54). The speed of AhR-degradation in macrophages was determined by western blot analysis (**Figure 1F**). Both treatments, with 2 μ M BaP or 100nM FICZ, led to AhR-degradation. Half of the AhR



amount was degraded after 2.7h and 1.8h for BaP and FICZ, respectively. Notably, one-third of AhR was not degraded for both ligands within the investigated time frame, suggesting that this AhR fraction does not enter the nucleus and is subject to nuclear export and subsequent degradation.

It was previously shown, that most changes in protein abundances can be found 4h after AhR activation and earlier time points show few altered proteins (55), thus minimizing the potential impact of newly synthesized proteins on post-translational modification. Hence, 2h treatments were used to

investigate the participation of AhR-dependent post-translational modification in immunomodulation. After stimulation, cells were lysed, and the total proteome, ubiquitome, and phosphoproteome were analyzed utilizing label-free quantitative LC-MS/MS.

Proteomic Changes Induced by AhR-Ligands

First, the effects of AhR activation on the global proteome were investigated in endotoxin-stimulated macrophages. Alteration of

protein levels after stimulation with AhR-ligand with and without LPS was investigated for seven donors, resulting in 5327 identified proteins. A reliably quantified core proteome, meaning quantified in at least four replicates of one treatment, of 4336 proteins was defined for further analysis (**Supplementary Table 1**).

The stimulation with AhR-ligands led to a minimal number of significantly altered proteins ($p \leq 0.01$) after 2h (**Figure 2A**). BaP-treatment affected the abundance of five proteins. Three of them were up-regulated compared to the unstimulated control, and two were down-regulated. FICZ-treatment led to the down-regulation of 12 proteins and up-regulated eight. In contrast, LPS had a strong effect on the proteome. Roughly one-third of proteins were significantly affected after LPS, BL, and FL treatment (**Supplementary Figure 2**). At that, more proteins were down-regulated (18.5%) than up-regulated (13.5%) after LPS-treatment. A similar distribution was observed for BL (19.4% up, 15% down) and FL (17% up, 12.2% down). Interestingly, proteins regulated by stimulation with BaP and FICZ did not show any overlap, while most proteins were commonly regulated after stimulation with LPS, BL, and FL (**Figure 2B**). A total of 1251 proteins was altered under at least two of these conditions, with 772 being commonly regulated for all treatments. Next, pathway enrichment analysis was conducted to identify cellular processes affected by protein regulations. For LPS, FL, and BL-treatment, metabolism of RNA and proteins were most affected, reflecting the high number of regulated proteins (**Figure 2C**). Furthermore, processes of the (innate) immune response and ongoing infectious diseases were regulated (**Figure 2C**). The pathways enriched after FICZ treatment were mainly related to mRNA-translation. Due to the limited number of regulated proteins, no pathways were enriched in BaP-treated cells.

To analyze the immunomodulatory function of AhR under inflammatory conditions in more detail, the double-stimulated samples, BL and FL, were additionally compared to LPS-treated cells (**Figure 2D**). Although the number of differentially abundant proteins was small, five proteins were commonly affected by BL and FL compared to LPS alone (**Figure 2E**). The levels of SLAM family member 8 (SLAMF8) and Disintegrin and metalloproteinase domain-containing protein 17 (ADAM17) were decreased, whereas the levels of Ubiquilin-1 (UBQLN1), Cyclin-dependent kinase inhibitor 1 (CDKN1A), and Cytochrome P450 1B1 (CYP1B1) were increased (**Supplementary Figure 3**). Pathway enrichment analysis resulted in no significantly enriched pathways within the differentially abundant proteins comparing BL and LPS (**Figure 2F**). Proteins participating in the Tryptophan metabolism and Steroid hormone biosynthesis were enriched comparing FL and LPS-treated cells (**Figure 2F**). BaP metabolites can induce DNA damage through formation of adducts (56). Hence, the increase of CDKN1A levels, which is an inhibitor of cell cycle progression in response to DNA damage (57) and blocks M-CSF dependent macrophage proliferation in response to IL4 (58), was confirmed by western blot analysis (**Figure 2G**). Both, BL and FL, showed significantly increased CDKN1A

signals compared to LPS, suggesting a potential inhibition of macrophage *in situ* proliferation.

Taken together, AhR activation by BaP or FICZ had a limited effect on protein abundances after 2h. In contrast, LPS-stimulation regulated many proteins involved in RNA and protein metabolism and innate immune responses, reflecting the increased gene expression at the early activation status (59). However, the effects of co-stimulation with AhR-ligands were similarly limited as for stimulation with BaP or FICZ alone, suggesting only a minor role of AhR activation on the macrophage proteome after 2h. Hence, non-genomic signaling by AhR might be responsible for the observed reduction of TNF expression and release.

AhR-Stimulation Affects Ubiquitination of Multiple Proteins in Macrophages

Activation of AhR has been shown to alter ubiquitination and proteasomal degradation of proteins (20). Thus, we aimed to characterize the ubiquitination state of cellular proteins after AhR-stimulation by BaP or FICZ with and without LPS-treatment. Lysates of stimulated macrophages from nine healthy donors were pooled, digested, and peptides harboring the Ubiquitin-Remnant-Motif (K- ϵ -GG) were enriched and quantified by LC-MS/MS in duplicates.

In total, 5,975 ubiquitination-sites (Ub-sites) were quantified, and Ub-sites with a fold change ≥ 2.5 relative to the respective control were considered as altered (**Supplementary Table 2**) (**Supplementary Figure 4**). As for proteins, most alterations occurred in samples treated with LPS, regardless of co-stimulation with AhR-ligands (**Figure 3A**). Thereby, twice as many Ub-sites were increased than reduced in abundance in LPS-treated samples, whereas such a difference was not observed after treatment with AhR-ligands alone (**Figure 3A**).

Most of the 90 Ub-sites altered by FICZ-treatment were affected by BaP, BL, or FL as well. Only ten sites were unaffected by all other treatments (**Figure 3B**). In contrast, 64% of Ub-sites altered by BaP-treatment were specific to this treatment. The overlap of altered Ub-sites after stimulation with LPS, BL, and FL was similar to the overlap of regulated proteins. A total of 490 Ub-sites was altered under at least two of these conditions, with 269 commonly regulated for all treatments (**Figure 3B**). About 10 to 20% of the Ub-site-alterations under one condition were unique for this treatment.

Comparing ubiquitination after double-stimulation to LPS-treated cells, FICZ affected more than 3-times more Ub-sites than BaP (**Figure 3C**). Thereby, increase and decrease of abundance occurred at the same frequency for both ligands. 22 Ub-sites were commonly altered for BL and FL compared to LPS (**Figure 3D**).

Stimulation of macrophages with LPS leads to activation of the Toll-like receptor 4 (TLR4) (60). Activation of TLR4 has been shown to trigger three signaling axes: The PI3K-Akt signaling, the MyD88-dependent, and the MyD88-independent pathway. As part of the MyD88 dependent signaling cascade, the ubiquitination of multiple proteins is essential for the signaling cascade (61). In our experiments, MyD88, TRAF6, NEMO, and

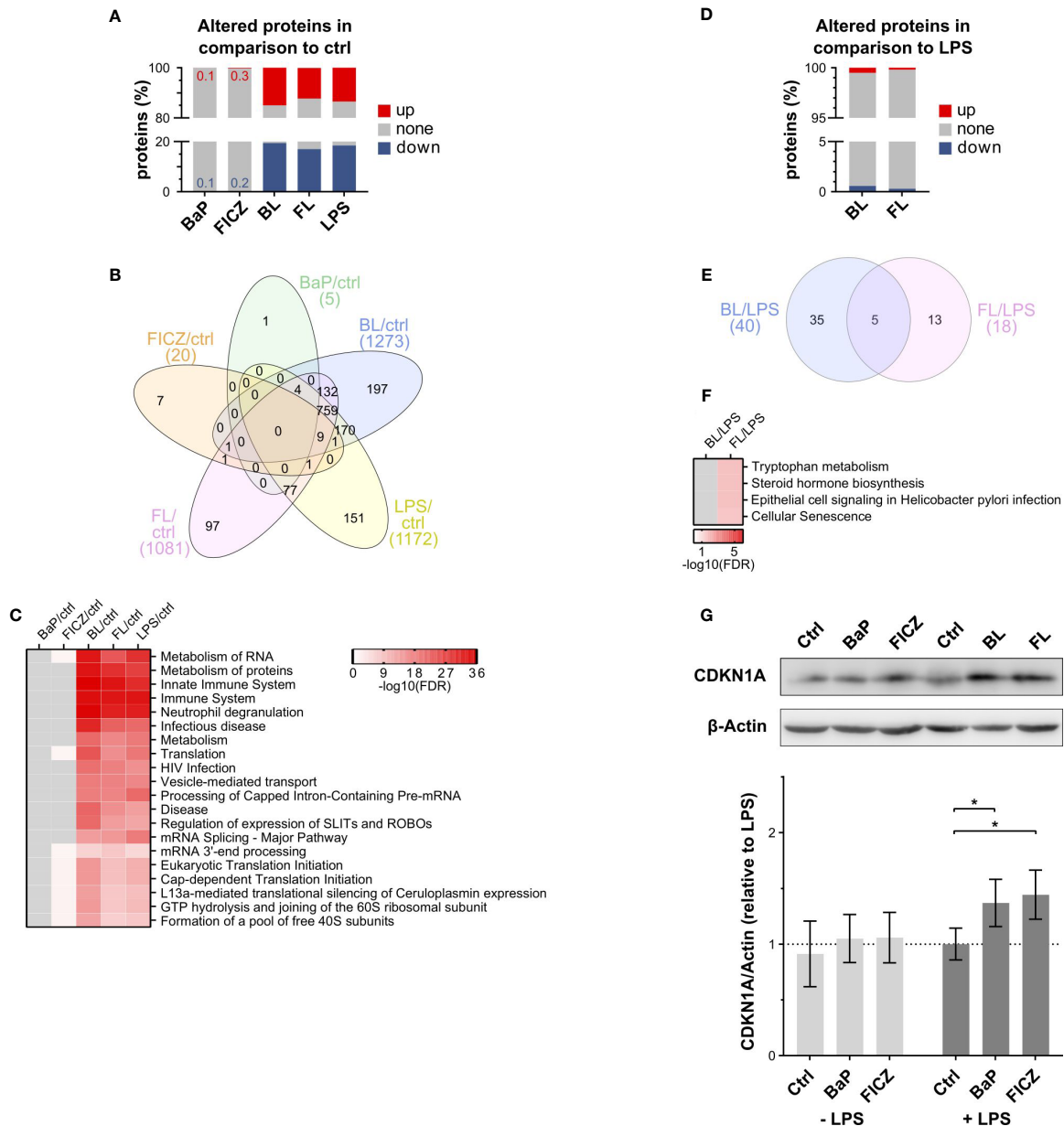


FIGURE 2 | Proteomic analysis of AhR-ligand treated macrophages in the presence/absence of LPS. **(A)** Percentage of significantly altered proteins after 2h compared to DMSO (ctrl). Proteins were considered as significantly altered compared to the control with a p -value ≤ 0.01 , as determined by Student's t -test ($n = 7$). **(B)** Overlap of altered proteins between treatments. **(C)** Pathways enriched among regulated proteins compared to the unstimulated control. Pathway enrichment analysis was conducted using the DAVID bioinformatics resources against KEGG and Reactome reference databases. Shown are the top 10 pathways based on their false discovery rate (FDR) for each treatment. **(D)** Percentage of significantly altered proteins in ligand- and LPS-stimulated cells in comparison to LPS alone (p -value ≤ 0.01 , $n = 7$). **(E)** Overlap of proteins altered by AhR-ligands under inflammatory conditions. **(F)** Pathways enriched among regulated proteins in BL- and FL-treated cells compared to LPS-treatment. Shown are all significantly enriched pathways (FDR ≤ 0.05). (BL: BaP+LPS-treated; FL: FICZ+LPS-treated) **(G)** Relative CDKN1A protein levels were determined by western blot analysis. CDKN1A signal intensities were normalized to β -Actin. Shown is one representative blot out of 6 independent experiments and donors and normalized intensities relative to LPS-treatment \pm SEM ($n = 6$). Significant changes were determined by two-sided, paired t -test ($*p \leq 0.05$).

$\text{I}\kappa\text{B}\alpha$ were found ubiquitinated, with NEMO and $\text{I}\kappa\text{B}\alpha$ being ubiquitinated at two sites (**Figure 3E**). All six Ub-sites were up-regulated upon LPS-treatment. The strongest increase was found for the ubiquitination of $\text{I}\kappa\text{B}\alpha$ at Lysine 98 ($\text{I}\kappa\text{B}\alpha_{98}$), which was

more than 8-times increased. This up-regulation was independent of co-stimulation with BaP or FICZ. $\text{I}\kappa\text{B}\alpha_{238}$ exhibited the highest difference between double-stimulated (BL or FL) and LPS-treated cells (1.75x FL/LPS and 1.45x BL/LPS).

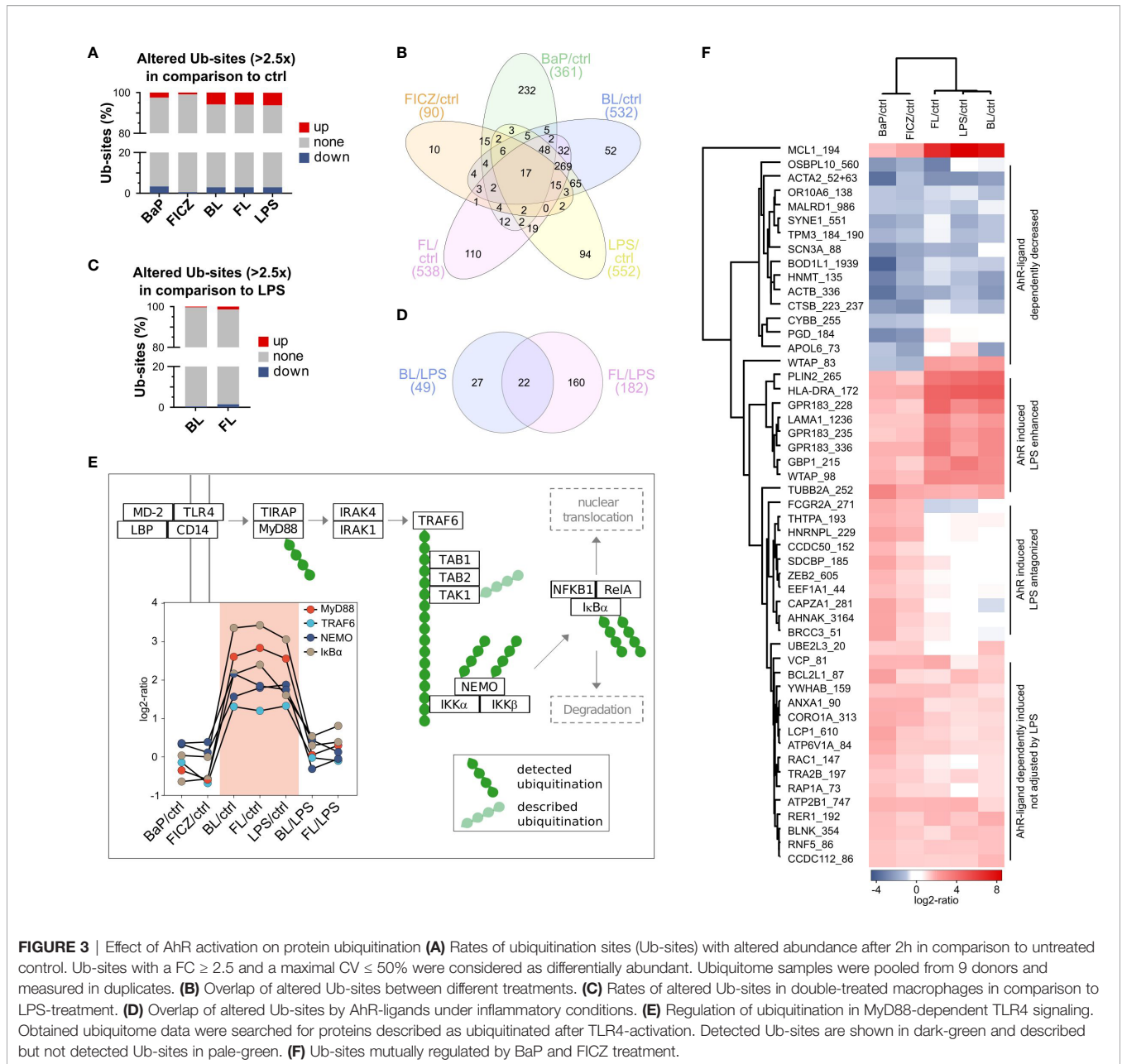


FIGURE 3 | Effect of AhR activation on protein ubiquitination **(A)** Rates of ubiquitination sites (Ub-sites) with altered abundance after 2h in comparison to untreated control. Ub-sites with a FC ≥ 2.5 and a maximal CV $\leq 50\%$ were considered as differentially abundant. Ubiquitome samples were pooled from 9 donors and measured in duplicates. **(B)** Overlap of altered Ub-sites between different treatments. **(C)** Rates of altered Ub-sites in double-treated macrophages in comparison to LPS-treatment. **(D)** Overlap of altered Ub-sites by AhR-ligands under inflammatory conditions. **(E)** Regulation of ubiquitination in MyD88-dependent TLR4 signaling. Obtained ubiquitome data were searched for proteins described as ubiquitinated after TLR4-activation. Detected Ub-sites are shown in dark-green and described but not detected Ub-sites in pale-green. **(F)** Ub-sites mutually regulated by BaP and FICZ treatment.

Thus, AhR activation did not interfere with ubiquitination in MyD88-dependent TLR4-signaling.

Next, we asked which ubiquitinations were concurrently altered after AhR-stimulation. Therefore, we filtered for Ub-sites, which were consistently ≥ 2.5 -times more or less abundant in BaP and FICZ-treated samples than in the unstimulated control. Of 51 mutually affected Ub-sites in 48 proteins, 36 Ub-sites were more abundant in BaP- and FICZ-treated macrophages as in unstimulated control cells, whereas 15 Ub-sites had a decreased abundance. Cluster analysis of these Ub-sites revealed three distinct groups of AhR-ligand dependently induced ubiquitination concerning their response to LPS: (1) induction not affected by LPS, (2) antagonized by LPS, and (3) LPS-enhanced induction (**Figure 3F**). However, such clustering was not observed for AhR-

ligand dependently reduced Ub-sites. While LPS induced most of the Ub-sites in group 1 to a similar degree, ubiquitination of Ras-related protein Rac1 (RAC1_147) and Ras-related protein Rap-1A (RAP1A_73) was not induced by LPS alone. Thus, the Ub-sites RAC1_147 and RAP1A_73 were the only sites induced by both AhR-ligands completely independent of LPS. Interestingly, both proteins exhibit GTPase-activity (62), indicating modulation of small GTPase-activity as a potential mechanism of non-genomic AhR-signaling.

Pathway enrichment analysis for the set of proteins ubiquitinated mutually regulated was conducted utilizing DAVID against the KEGG pathway database. Four pathways were significantly enriched (FDR ≤ 0.05): Phagosome, Osteoclast differentiation, Viral myocarditis, and PI3K-Akt signaling

pathway (**Supplementary Figure 5**). With seven proteins (ACTB, ATP6V1A, CORO1A, TUBB2A, RAC1, FCGR2A, HLA-DRA), the highest number of proteins participates in phagosomal processes. Five proteins (LAMA1, MCL1, RAC1, YWHAB, BCL2L1) were associated with the PI3K-Akt signaling pathway, one of the signaling axes of activated TLR4.

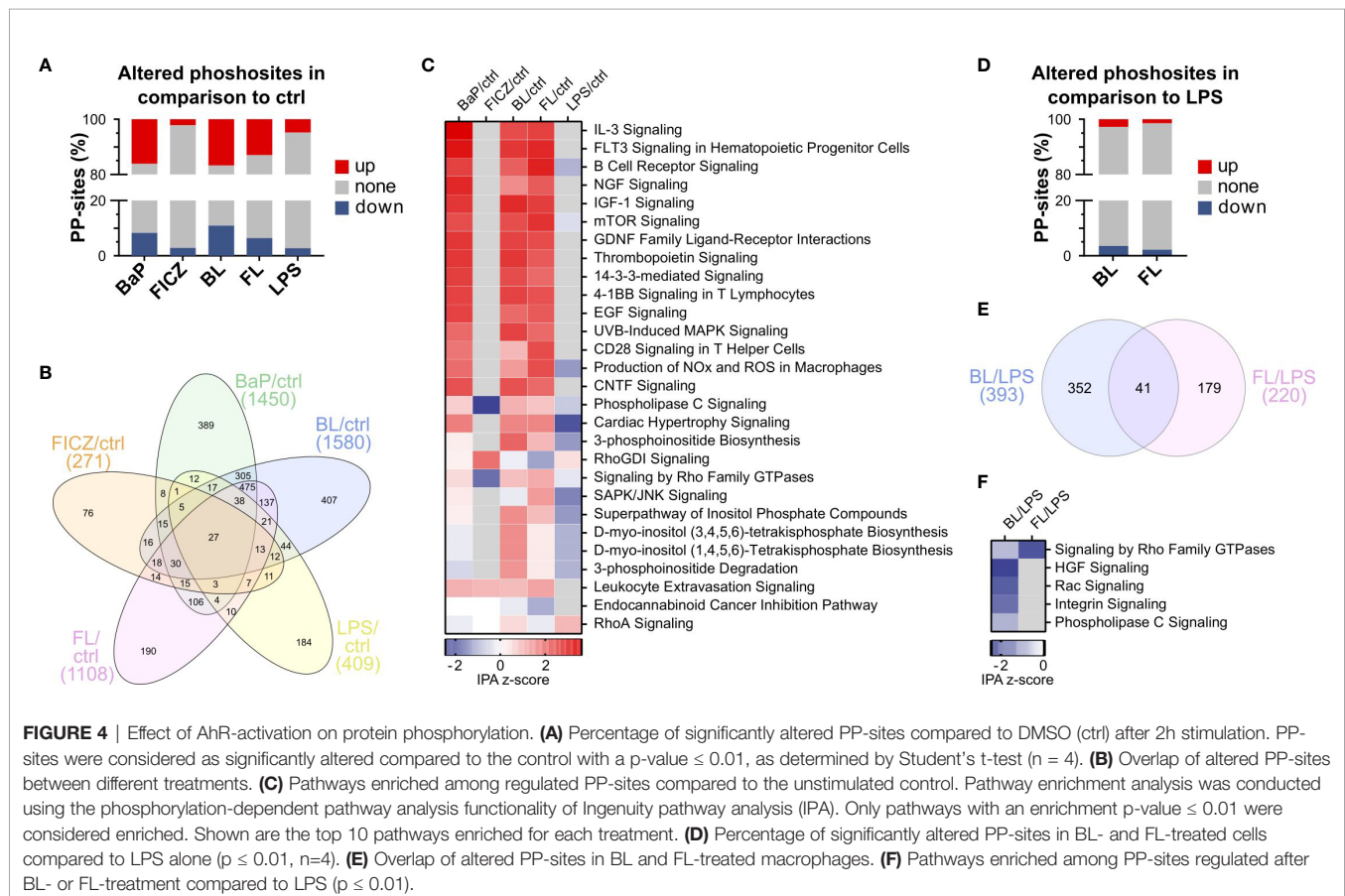
Our ubiquitome data showed that AhR-activation did not interfere with Ub-dependent processes in MyD88-dependent TLR4-signaling. LPS-treatment dominated most regulations of Ub-sites. However, with RAP1A_73 and RAC1_147, two Ub-sites in GTPases were AhR-ligand-dependently, and LPS-independently induced. Both proteins participate in phagocytosis, and RAC1 participates in PI3K-Akt signaling as well. These two pathways were enriched among differentially ubiquitinated proteins after AhR activation, indicating a regulatory role of the RAC1-PI3K-AKT signaling pathway and affected phagocytosis.

Effect of AhR-Stimulation on Protein Phosphorylation Is Ligand-Specific

Many biological processes, including the RAC1-PI3K-AKT signaling pathway, are regulated by protein phosphorylation, which influences protein activity. AhR activation can affect protein-phosphorylation, e.g., by releasing SRC from the cytoplasmic AhR-complex (14). Thus, the phosphorylation state

of cellular proteins was analyzed next. Again, macrophages were stimulated with BaP or FICZ alone or in combination with LPS for 2h. Phosphorylated peptides were enriched by complementary use of TiO₂ and Fe-NTA based affinity chromatography from digested lysates of macrophages from 4 healthy donors.

In total, 17,089 phosphorylation-sites (PP-sites) were identified. 9,742 PP-sites were reliably quantified in at least 3 of 4 replicates in one condition, with more than 5,400 sites for each condition (**Supplementary Table 3**). About 4,000 PP-sites were quantified in all six conditions. Significantly altered PP-sites were identified by Student's t-test. The threshold for significant alteration was set at $p \leq 0.01$ (**Supplementary Figure 6**). The most distinct alterations were found in BaP-treated samples (**Figure 4A**). BaP-treatment altered 24%, and BaP in combination with LPS-stimulation altered 26% of PP-sites compared to the unstimulated control. In contrast, FICZ-treatment and LPS-stimulation affected 5% and 7%, respectively. The combination of both stimuli altered 18% of PP-sites. All treatments, except FICZ, led to markedly more up-regulated than down-regulated PP-sites. A high overlap of 912 PP-sites was regulated by BaP and BL, while the two treatments showed only 389 and 407 unique PP-sites (**Figure 4B**). Only minor fractions were shared by only one of these treatments and FICZ, FL, or LPS. In contrast, the overlap in regulated PP-sites was less distinct for FICZ containing treatments. While FL



affected four times more sites than FICZ, only 48% of FICZ-regulated PP-sites were shared with FL. BL mutually affected 69% of FL-regulated sites. However, LPS-treatment resulted in 51% of regulations being observed for at least BL or FL.

Next, signaling pathways affected by AhR-activation-dependent phosphorylations were identified using the phosphorylation pathway analysis function of Ingenuity Pathway Analysis (IPA). IPA identifies overrepresented pathways within differentially phosphorylated proteins and predicts pathway activity based on PP-site regulations (IPA z-scores). Pathways with an enrichment p-value ≤ 0.01 and absolute z-score ≥ 1 were considered as significantly altered. This approach identified 28 pathways significantly altered for at least one treatment (**Figure 4C**). Most of these pathways were activated (z-score ≥ 1) rather than deactivated (z-score ≤ -1). Interestingly, BaP, BL, and FL had a similar effect on the pathway level. Activation was most pronounced for IL-3 Signaling (z-score = 3.6) and FLT3 Signaling (z-score = 3.3) after BaP-treatment. Leukocyte Extravasation Signaling was the only pathway activated by all treatments with AhR-ligands (**Figure 4C**).

In contrast to the marked effects of BaP, BL, and FL, the effect of FICZ was limited (**Figure 4C**). Our data revealed that FICZ deactivated Phospholipase C Signaling and Signaling by Rho Family GTPases. In line with that, signaling by Rho GDP-dissociation inhibitor (RhoGDI Signaling), which negatively regulates Rho-family GTPases, was enhanced. Interestingly, LPS-treatment exhibited a deactivating effect on phosphorylation-dependent signaling after 2h of stimulation. None of the pathways activated after BL and FL treatment was enhanced after LPS-stimulation. RhoA Signaling was the only pathway that was activated by LPS (z-score = 1).

Comparing BL- and FL-stimulated with LPS-stimulated macrophages, 6% and 4% of PP-sites were regulated (**Figure 4D**). Up- and down-regulation appeared at nearly the same frequencies. The overlap of regulated sites for BL and FL was limited to 41 of 220 sites (**Figure 4E**).

Next, we determined AHR-induced phosphorylation-dependent signaling pathways altered in BL- or FL treated cells compared to LPS-stimulation (**Figure 4F**). Five pathways were affected by BL-treatment: HGF, Rac, Integrin, and Phospholipase C Signaling, and Signaling by Rho Family GTPases, which was the only pathway likewise affected by FL-treatment. All pathways were attenuated in double-stimulated macrophages. Our ubiquitome results showed increased ubiquitination of RAC1 after AhR activation, suggesting that this ubiquitination has mitigated Rac Signaling. Notably, Rac signaling cascades are also part of HGF and Integrin Signaling, indicating that attenuation of Rac Signaling can lead to the observed attenuation in HGF and Integrin Signaling.

Taken together, BaP, as well as double-stimulation with BL or FL, strongly regulated protein-phosphorylation, in contrast to FICZ or LPS. Enrichment analysis revealed that most pathways were activated after BaP-, BL-, or FL-treatment, whereas LPS had an attenuating effect on phosphorylation-dependent signaling. Comparing BL and FL to LPS-stimulation, all enriched pathways

were attenuated. Most of these pathways depend on Rac or RhoGTPases, indicating a central role of these proteins for AhR-dependent effects.

Altered Kinase Activities After AhR Activation

Next, we aimed to determine which kinases exhibit an altered activity after AhR activation and are thus likely responsible for the observed changes in protein phosphorylation. For this purpose, kinase activities were inferred by integrating amino acid sequence windows of significantly altered PP-sites with kinase-substrate motifs utilizing the KinSwingR package for the R environment for statistical computing (50), generating a normalized and weighted score for the predicted kinase activity (SWING). Additionally, the probability (p) for observation of other kinases with higher or lower SWING scores was calculated. Only kinases with $p \leq 0.05$ were considered as significantly regulated.

In total, 53 kinases were found differentially active after at least one treatment compared to unstimulated control samples (**Figure 5A**). Thereby, LPS and FICZ-stimulated macrophages exhibited similar patterns of kinase activity. This extended to BaP-, BL-, and FL-stimulated cells and resembled the pattern observed for the regulation of signaling pathways (**Figure 4C**). Interestingly, SRC, which is part of the cytosolic AhR-complex (14), appeared to be deactivated after BL-, FL-, and especially BaP-treatment (SWING = -1.9). The most distinct activation was inferred for PRKACA after FL-treatment (SWING = 6.7). PRKACA was likewise activated by BL and BaP, although to a lesser degree. In contrast, PRKACA was less active after FICZ-treatment and unaffected by LPS alone. The most distinct deactivation was inferred for CSNK2A1 after BaP-treatment (SWING = -4.6). Noteworthy, treatment with LPS or FICZ resulted in the attenuation of protein kinase C (PKC) activity. Five PKC isoenzymes (PRKCA, PRKCB, PRKCD, PRKCE, PRKCF) had reduced activity after both treatments. In contrast, all of these were unaffected by BL, FL, and BaP, with the exceptions of reduced PRKCE activity after BL-treatment and slightly increased PRKCA activity after BaP-treatment.

Comparing BL- and FL-treated with LPS-treated cells, inferred activity was altered for 30 kinases (**Figure 5B**). Noticeably, regulations for most kinases were opposite for BL and FL. IGF1R and PRKG2 are the only kinases commonly more active after double-treatment compared to LPS alone. HIP1L2, CDK9, MAPK1, and PRKDC are commonly less active, although the deactivation was markedly lower for BL.

Taken together, our ubiquitome and phosphorylation-dependent pathway analysis indicated alterations in RAC signaling. It was shown before, that signaling by RAC1 after TLR4 activation induces AKT serine/threonine kinase (AKT)-activity (63). Thus, changes in AKT-activity were further examined. The AKT isoforms AKT1 and AKT2 were both less active in BL-treated macrophages than after LPS-treatment (**Figure 5B**). Both kinases seemed activated after FL-treatment. However, the probability for kinases with higher SWING scores did not fulfill the significance threshold. 26 significantly altered PP-sites in 21 phosphoproteins were mapped to AKT1/2 after BL-

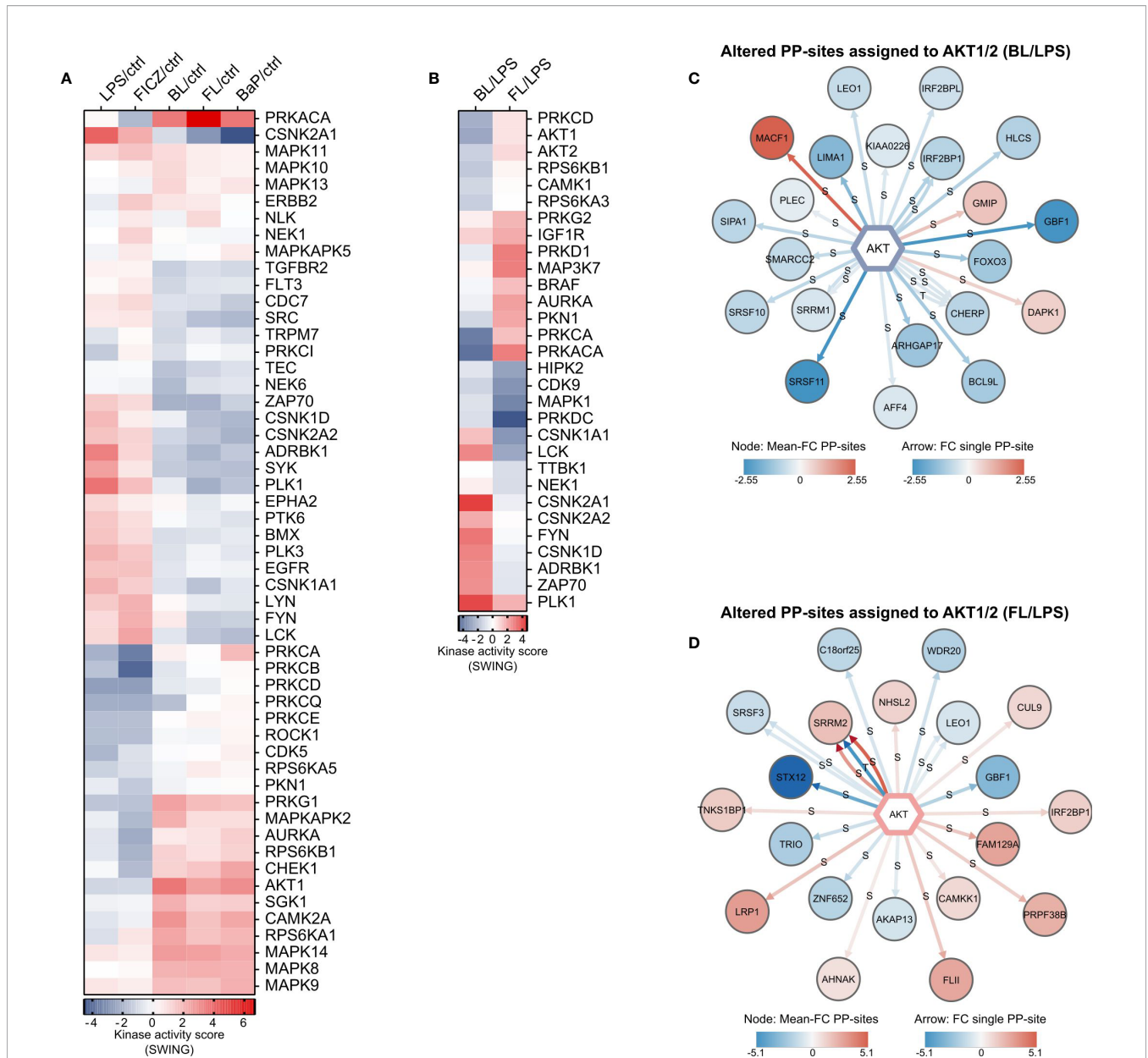
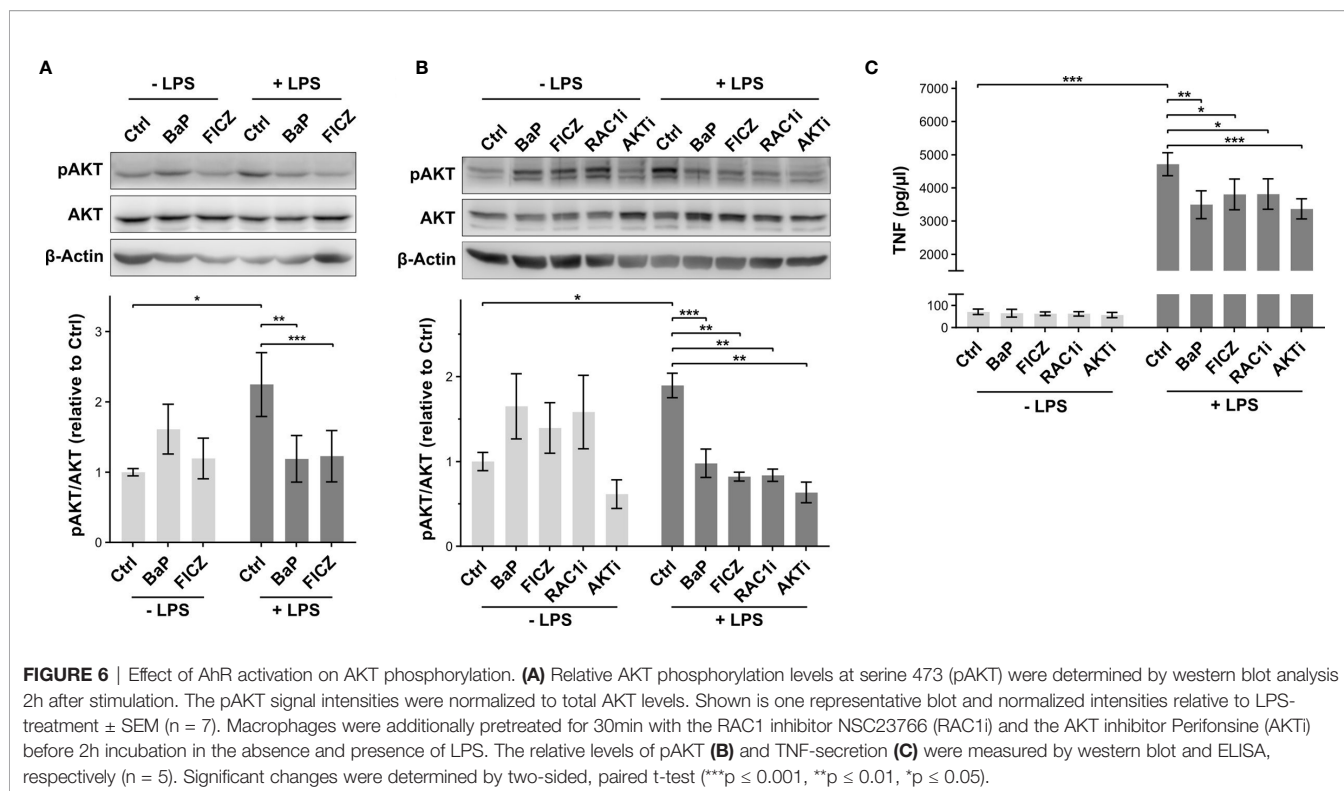


FIGURE 5 | Inferred kinase activities and substrates. **(A)** Inferred alterations in kinase activities responsible for altered PP-sites in comparison to untreated cells, and **(B)** altered PP-sites in BL- or FL-treated macrophages compared to LPS-treated cells. Kinase-substrate motifs were calculated based on the kinase-substrate dataset from PhosphoSitePlus. Relative kinase activity scores (SWING) were calculated by integrating amino acid sequence windows of significantly altered PP-sites with kinase-substrate motifs utilizing KinSwingR. Altered phosphorylations in BL- **(C)** and FL- **(D)** treated cells compared to LPS-treatment assigned to AKT1/2. Data on regulated PP-sites assigned to AKT serine/threonine kinase (AKT) isoforms 1 and 2 were extracted after sequence-motive assignment. Each arrow represents a single PP-site. The color of the kinase target represents the mean FC over all assigned PP-sites.

treatment (**Figure 5C**). Of these sites, three were more abundant, while 23 PP-sites were down-regulated, indicating the reduced AKT activity after BL-treatment. Of the PP-sites with altered abundance after FL-treatment, 24 sites in 20 proteins were assigned to AKT1/2 (**Figure 5D**). Half of these were more, the other 12 were less abundant in FL-treated than in LPS-treated cells. Thus, AKT-activity was found decreased by BL-treatment and unaffected by FL-treatment compared to LPS-stimulation based on inference of kinase activity from the phosphoproteome data.

To validate the effect of BL on AKT-activity, the phosphorylation of AKT at serine 473 (pAKT) was analyzed by phosphosite specific western blot. The resulting intensities for pAKT were normalized to the total AKT signal (**Figure 6A**). As expected, LPS-treatment increased the pAKT level in macrophages. This induction was not found after co-treatment with BaP or FICZ, indicating a suppressive effect of the AhR-ligands on AKT activation. Next, the dependence of AKT phosphorylation on RAC1 activation was investigated utilizing a RAC1 specific inhibitor. Analysis of pAKT levels after



RAC1-inhibition indicates that AKT-activity is diminished to a degree comparable to BL- and FL-treatment (**Figure 6B**). Direct inhibition of AKT led to a more distinct attenuation. The release of TNF was analyzed for the same set of samples (**Figure 6C**). Both, inhibition of RAC1 and AKT, led to a decrease in TNF-release after LPS-treatment comparable to the effect of the AhR-ligands BaP and FICZ.

The inference of kinase activity endorsed the ligand dependency of AhR induced regulations seen in the phosphoproteome data. At it, AKT, a downstream signaling component in RAC1-dependent TLR4 signaling, was attenuated after BL-treatment compared to LPS. The AKT-activating Rac signaling was attenuated by BL, as observed in our phosphoproteome. Inhibition of RAC1 reduced AKT phosphorylation in response to LPS-treatment. The reduced AKT phosphorylation was associated with a reduction of TNF-release.

DISCUSSION

The AhR has important immunomodulatory properties, such as limiting the release of pro-inflammatory cytokines and protection from septic shocks, and can signal through genomic and non-genomic mechanisms (2, 9, 10, 19). Likewise, a decrease in the release of pro-inflammatory TNF was observed in this study and previously described (25). However, molecular mechanisms are not fully understood. Using a multi-PTM-omics approach, we unraveled the mechanisms of non-genomic AhR-signaling in immunomodulation. The alterations of protein abundance, ubiquitination, and phosphorylation after

treatment with the endogenous AhR-ligand FICZ and exogenous ligand BaP were analyzed in endotoxin-stimulated human monocyte-derived macrophages. Furthermore, kinase-activities were inferred from our phosphoproteome results.

Limited Response by Altered Protein Abundance

The effect of AhR activation on protein abundance observed in this study was minute. Treatment with AhR-ligands (BaP or FICZ) alone led to no commonly regulated proteins, while five were commonly regulated after co-stimulation with LPS. Such a limited response to BaP after short incubation time (2h) was previously described for the murine hepatoma cell line Hepa1c1c7, where alterations in protein levels peaked after 4h and 24h (55). To our knowledge, no transcriptome dataset matching cell type and stimulation used in this study is available yet. Though, Sparfel et al. demonstrated that, after 8h of BaP-exposure, 96 genes are differentially expressed in human macrophages, while 1100 genes are affected after 24h (64). Together, these data suggest that AhR-dependent alteration in protein level has a later onset than 2h after ligand-treatment, indicating regulations of protein ubiquitination and phosphorylation depend rather on non-genomic mechanisms than induced protein expression by the transcriptional activity of AhR.

Immunomodulation on the TLR4-RAC1-PI3K-AKT Axis

Regulation of protein activity through modifications like ubiquitination and phosphorylation is typically faster than

regulation through protein abundance. In addition, PTM-dependent signaling cascades are often responsible for altered gene expression. Signaling of LPS-triggered TLR4 *via* the canonical MyD88-dependent pathway essentially depends on the ubiquitination of multiple proteins (61). All ubiquitinations involved in MyD88-dependent TLR4-signaling identified in this study were increased after LPS-stimulation, indicating a sustained TLR4-activation. AhR activation by BaP or FICZ did not affect these ubiquitinations. Merely, the ubiquitination of I κ B α was slightly increased after double-stimulation. Hence, non-genomic AhR-signaling seems not to modulate MyD88-dependent TLR4-activation through altered ubiquitination.

Consequently, we focused on ubiquitinations mutually regulated by both AhR-ligands to identify Ub-dependent signaling events modulated directly by AhR acting as an integral component of an E3 ubiquitin ligase complex or indirectly after AhR activation. Most of the 36 Ub-sites induced by AhR activation were enhanced, antagonized, or induced to a similar degree by LPS-treatment. Only two Ub-sites, RAC1_147 and RAP1A_73, were up-regulated by BaP and FICZ completely independent of LPS-treatment. Besides interfering signaling cascades, an explanation for the antagonization of AhR-dependent ubiquitination by LPS relies on the strong induction of protein ubiquitination by LPS. A strong increase of poly-ubiquitinations leads to limitations in the pool of free ubiquitin, which results in a deprivation of Ub from other ubiquitinations, especially mono-ubiquitinations (65–67).

Interestingly, the ubiquitination of RAP1A at Lysine 73 was previously not described and not listed in the PhosphoSitePlus or BioGRID database (51, 68). RAP1A protein levels did not decrease after BaP or FICZ-treatment, indicating non-degradative ubiquitination. Shao et al. reported a negative regulation RAP1A-activity through an E3 ubiquitin-protein ligase CBL (CBL)-dependent, but proteolysis-independent mechanism (69). AhR activation by tetrandrine activates CBL in an SRC-dependent, non-genomic manner. This activation leads to ubiquitination and degradation of Tyrosine-protein kinase SYK (22). The SRC-activity inferred from our phosphoproteome did not increase after AhR activation. However, phosphoproteome and ubiquitome were analyzed after 2h treatment, whereas SRC-activation is an initial event after AhR activation. The initially increased SRC-activity decreases by 50 % within the first 25 min after AhR-ligand administration (70). In macrophages, RAP1A is required for Fc gamma receptor-dependent phagocytosis (71). Additionally, RAP1A activation fosters superoxide generation during phagocytosis of IgG-opsonized zymonans, mechanistically involving the release of RAC1 from the RAC1-RhoGDI complex (72).

The ubiquitination of RAC1 at its major ubiquitination site K147, which is the Ub-site regulated in this study, is dependent on the activity of c-Jun N-terminal kinases (MAPK8, MAPK9, MAPK10) (73). The kinase activity of MAPK8 and MAPK9 was markedly increased by BaP-treatment and double-stimulation with LPS and AhR-ligand. The activity increase was smaller for FICZ. The same was observed for MAPK10, although to a lesser

extent. The lower increase of MAPK8/9/10-activity after FICZ-stimulation is in line with a less distinct up-regulation of the observed RAC1-ubiquitination. Therefore, the increased RAC1_K147-ubiquitination is likely dependent on AhR-induced activity of the c-Jun N-terminal kinases JNK. RAC1 links TLR-activation to the PI3K-Akt signaling pathway contributing to pro-inflammatory signaling in macrophages after LPS-encounter (74, 75). The increased ubiquitination potentially interferes with this activation pathway, which is additionally supported by further components of PI3K-AKT-signaling (LAMA1, MCL1, YWHAB, BCL2L1) being ubiquitinated after AhR activation. In line, Rac Signaling was found to be decreased in BL-stimulated macrophages compared to LPS-activation alone.

These cells likewise showed a decrease in AKT-activity based on kinase activity inference from the phosphoproteome data. The decreased AKT-activity could be confirmed by western blot analysis of the activation-dependent AKT phosphorylation at serine 473. Differing from the prediction by kinase activity inference, AKT activity was found attenuated for BL and FL compared to LPS. The kinase activity inference is based on sequence windows of significantly altered PP-sites mapped to kinase-substrate motifs (50). Likely, inference of kinase activity was more precise due to the broader data basis of regulated phosphorylation sites for BL than FL (393 versus 220). Utilizing a RAC1-specific inhibitor (76), the decreased pAKT-levels in BL- and FL-treated cells were mimicked in this study, confirming that a decreased RAC1-activity leads to decreased AKT-activity in LPS-treated macrophages. Inhibition of RAC1 or AKT led to an attenuated TNF-release after LPS-stimulation similar to the co-treatment with the AhR-ligands BaP or FICZ. In sum, these findings indicate that AhR-activation attenuates the TLR4-RAC1-PI3K-AKT axis.

In addition to the connection of TLR4-activation to the PI3K-Akt signaling pathway, RAC1 has been shown to link LPS-stimulation and the formation of reactive oxygen species (ROS), which stimulates NF- κ B activation and subsequent TNF-secretion (74). In this process, RAC1 is required for the recruitment of the NADPH oxidase activating subunit neutrophil cytosol factor 2 (NCF2 or p67^{phox}) to the membrane of phagocytes (77) and to keep NCF2 in the active conformation (78). Based on our data, it is not possible to exclude an effect of BaP or FICZ on the RAC1-dependent activation of NADPH oxidases. Nevertheless, the finding that inhibition of AKT led to a decrease in TNF-secretion comparable to the effect of the AhR-ligands is an indicator for a subsidiary role of an altered RAC1-dependent NADPH oxidase activity at the investigated time point and ligand concentrations.

Besides providing a second route for I κ B α -phosphorylation after TLR4-activation, AKT phosphorylates additional targets like BAD, TSC2, and CREB, thereby directly impacting macrophage survival, polarization, and autophagy (79, 80). One of these additional targets is Forkhead box protein O3 (FOXO3), which was found less phosphorylated in BaP- and BL-treated cells. The result of this phosphorylation is the inhibition of the transcription factor FOXO3 (81), suggesting an enhanced

activity of FOXO3 after AhR activation by BaP. The inhibition of FOXO3 after TLR4 activation typically results in suppressed autophagy (82). In addition, AKT-dependent inhibition of FOXO3 through phosphorylation enhances the production of the anti-inflammatory cytokine IL-10 (83). Therefore, decreased FOXO3-phosphorylation would suppress IL-10 levels. In contrast, AhR activation is thought to increase IL-10-expression through SRC-dependent signaling (26). The balance of these two competing pathways may have an important role in AhR immunomodulatory functions.

Taken together, our data suggest that AhR activation by BaP induces JNK-dependent RAC1-ubiquitination, which inhibits the RAC1-PI3K-AKT-signaling axis after TLR4-activation and thus potentially contributes to the AhR-dependent attenuation of pro-inflammatory signaling in a non-genomic manner (Figure 7).

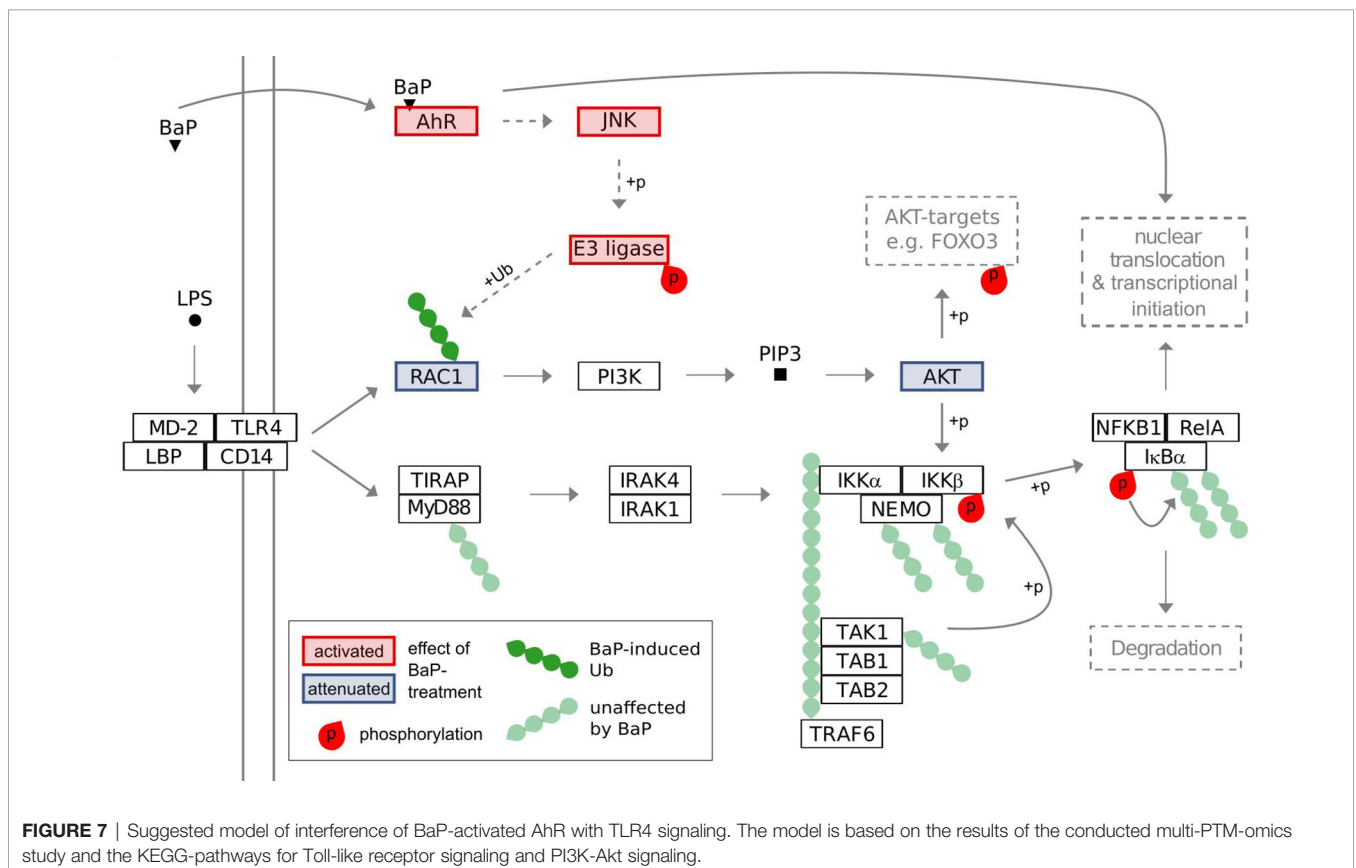
The Non-Genomic Immunomodulatory Response to AhR Activation Is Ligand-Dependent

The inhibitory effects of AhR-stimulation on Rac Signaling and AKT-activity in our phosphoproteome dataset were mainly observed for BaP-treatment. In contrast, FICZ did not alter Rac signaling but showed a comparably decreased AKT phosphorylation in western blot analysis. Although the used concentrations of BaP and FICZ led to comparable genomic responses as demonstrated by similar up-regulation of CYP1B1

and AHRR mRNA-expression, the non-genomic consequences differed. About 5-times more Ub- and PP-sites were regulated after BaP-treatment than after FICZ-administration. However, the differences diminished in macrophages treated with BaP or FICZ combined with LPS. Especially phosphorylation-dependent signaling and kinase-activities compared to LPS-treated macrophages were still divergent.

Different responses by the immune system to different AhR-ligands have been previously reported. TCDD induces differentiation of functional regulatory T cells, which suppress experimental autoimmune encephalomyelitis, whereas FICZ leads to T_H17 cell differentiation, which worsen disease progression in the same model system (84). Prolonged AhR activation with FICZ does not affect neutrophil recruitment or inducible nitric oxide synthase levels in a mouse model of influenza virus infection. In contrast, both are augmented by TCDD-treatment (85). It is suggested that the duration of AhR activation is a primary factor of AhR-ligand effects on the immune system (86). While TCDD is persistent with long *in vivo* half-life, FICZ is rapidly metabolized, requiring AhR-dependently expressed CYP1A1 and CYP1B1 (87, 88). After 5h, nearly no FICZ remains after the treatment of HepG2 cells (89). BaP, the exogenous ligand used in this study, is degraded likewise and metabolized nearly completely 24h after administration (55).

The induction of the metabolizing enzymes was not yet observable after 2h treatment, which was used in this study. Nevertheless, the induction was clear on the mRNA level after 6h, indicating that ligand-degradation did not take part at the



analyzed time-point. More likely, the structure of the ligands influences non-genomic AhR-dependent immunomodulation. Such a relation is known for other ligand-activated nuclear receptors, as reviewed by Jin and Li (90). The binding of structurally differing ligands results in different conformational states of the receptor, which then favors the binding of other proteins (90). Furthermore, a relation between structural ligand-properties and the results of AhR activation was previously described (91). Differences in ligand-binding-properties are sufficient for developing AhR-ligand-specific antagonists like the TCDD-antagonist CH223191 (92).

Both the higher persistence and different conformational changes after BaP-binding to AhR potentially contribute to the BaP-specific effects on protein ubiquitination and phosphorylation. However, through targeting AKT-activity, the effects of BaP and FICZ converged regardless of the differences in the phosphoproteome analysis. Finally, the mechanisms underlying the observed ligand-specific responses are not clear yet and need further investigations. In this study, FICZ, a UV light-dependent Tryptophan product, was investigated as endogenous AhR-ligand. Further Tryptophan-metabolites have been shown to activate or antagonize AhR, with many being derived from the intestinal microbiota (93). At the origin of these ligands, AhR is essential for intestinal immunity and barrier function (94, 95). Therefore, further endogenous ligands may be taken into account to better understand AhR-functions under physiological conditions and diseases. Moreover, considering the BaP-specific effects and the attenuation of LPS-dependent macrophage activation, BaP might act as a modulator of the microbiome-host interaction.

Conclusions

In this study, the non-genomic AhR-signaling and its role in immunomodulation were investigated. Therefore, alterations in protein abundance, ubiquitination, and phosphorylation were globally addressed utilizing respective omics approaches before the visibility of genomic signaling on the protein level. The observed alterations in post-translational modifications exhibited a dependency on the administered AhR-ligand. Finally, inhibition of the RAC1-PI3K-AKT signaling-axis in TLR4-signaling after BaP- or FICZ administration was insinuated. The inhibitory mechanism involves AhR-dependent JNK-activity and subsequent RAC1-ubiquitination. Conclusively, the obtained data may prove a valuable resource for further elucidation of non-genomic AhR-signaling in immunomodulation and their potential for targeting in AhR-dependent pathologies, e.g., atherosclerosis and major depressive disorder or diseases associated to a disturbed intestinal immunity.

REFERENCES

- Poland A, Glover E, Kende AS. Stereospecific, high affinity binding of 2,3,7,8-tetrachlorodibenzo-p-dioxin by hepatic cytosol. Evidence that the binding species is receptor for induction of aryl hydrocarbon hydroxylase. *J Biol Chem* (1976) 251(16):4936–46. doi: 10.1016/S0021-9258(17)33205-2

DATA AVAILABILITY STATEMENT

The mass spectrometry proteomic data presented in the study are publicly available. This data can be found here: ProteomeXchange Consortium (<http://proteomecentral.proteomexchange.org>) via the PRIDE partner repository (96) with the dataset identifier PXD020770.

ETHICS STATEMENT

The studies involving human participants were reviewed and approved by Ethics Committee of the University of Leipzig (Ref. #079-15-09032015). The patients/participants provided their written informed consent to participate in this study.

AUTHOR CONTRIBUTIONS

Conceptualization: MB and KS. Methodology: HG and KS. Software: IK and HG. Investigation: HG and KW. Writing—original draft: HG and KS. Writing—review and editing: HG, KW, IK, MB, and KS. All authors contributed to the article and approved the submitted version.

FUNDING

This work was supported by the Helmholtz Association of German Research Centers. This study was supported by a grant of the Deutsche Forschungsgemeinschaft (DFG) TRR67Z4 to MB and HG.

ACKNOWLEDGMENTS

The authors thank Maj Schuster, Julia Howanski, and Celine Hertel for excellent technical assistance and Dr. Anne Großkopf for providing antibodies. Furthermore, we thank the UFZ-funded ProMetheus platform for proteomics and metabolomics for the support of this project.

SUPPLEMENTARY MATERIAL

The Supplementary Material for this article can be found online at: <https://www.frontiersin.org/articles/10.3389/fimmu.2021.620270/full#supplementary-material>

- Gutierrez-Vazquez C, Quintana FJ. Regulation of the Immune Response by the Aryl Hydrocarbon Receptor. *Immunity* (2018) 48(1):19–33. doi: 10.1016/j.immuni.2017.12.012
- Esser C, Rannug A. The aryl hydrocarbon receptor in barrier organ physiology, immunology, and toxicology. *Pharmacol Rev* (2015) 67(2):259–79. doi: 10.1124/pr.114.009001

4. Gasiewicz TA, Singh KP, Bennett JA. The Ah receptor in stem cell cycling, regulation, and quiescence. *Ann N Y Acad Sci* (2014) 1310:44–50. doi: 10.1111/nyas.12361
5. Smith BW, Rozelle SS, Leung A, Ubellacker J, Parks A, Nah SK, et al. The aryl hydrocarbon receptor directs hematopoietic progenitor cell expansion and differentiation. *Blood* (2013) 122(3):376–85. doi: 10.1182/blood-2012-11-466722
6. Goudot C, Coillard A, Villani AC, Gueguen P, Cros A, Sarkizova S, et al. Aryl Hydrocarbon Receptor Controls Monocyte Differentiation into Dendritic Cells versus Macrophages. *Immunity* (2017) 47(3):582–96.e6. doi: 10.1016/j.immuni.2017.08.016
7. Riemschneider S, Kohlschmidt J, Fueldner C, Esser C, Hauschildt S, Lehmann J. Aryl hydrocarbon receptor activation by benzo(a)pyrene inhibits proliferation of myeloid precursor cells and alters the differentiation state as well as the functional phenotype of murine bone marrow-derived macrophages. *Toxicol Lett* (2018) 296:106–13. doi: 10.1016/j.toxlet.2018.07.050
8. Fueldner C, Kohlschmidt J, Riemschneider S, Schulze F, Zoldan K, Esser C, et al. Benzo(a)pyrene attenuates the pattern-recognition-receptor induced proinflammatory phenotype of murine macrophages by inducing IL-10 expression in an aryl hydrocarbon receptor-dependent manner. *Toxicology* (2018) 409:80–90. doi: 10.1016/j.tox.2018.07.011
9. Kimura A, Naka T, Nakahama T, Chinen I, Masuda K, Nohara K, et al. Aryl hydrocarbon receptor in combination with Stat1 regulates LPS-induced inflammatory responses. *J Exp Med* (2009) 206(9):2027–35. doi: 10.1084/jem.20090560
10. Sekine H, Mimura J, Oshima M, Okawa H, Kanno J, Igarashi K, et al. Hypersensitivity of Aryl Hydrocarbon Receptor-Deficient Mice to Lipopolysaccharide-Induced Septic Shock. *Mol Cell Biol* (2009) 29(24):6391–400. doi: 10.1128/mcb.00337-09
11. Bessede A, Gargaro M, Pallotta MT, Matino D, Servillo G, Brunacci C, et al. Aryl hydrocarbon receptor control of a disease tolerance defence pathway. *Nature* (2014) 511(7508):184–90. doi: 10.1038/nature13323
12. Nguyen LP, Bradfield CA. The search for endogenous activators of the aryl hydrocarbon receptor. *Chem Res Toxicol* (2008) 21(1):102–16. doi: 10.1021/tx7001965
13. Gao J, Xu K, Liu H, Liu G, Bai M, Peng C, et al. Impact of the Gut Microbiota on Intestinal Immunity Mediated by Tryptophan Metabolism. *Front Cell Infect Microbiol* (2018) 8:13. doi: 10.3389/fcimb.2018.00013
14. Enan E, Matsumura F. Identification of c-Src as the integral component of the cytosolic Ah receptor complex, transducing the signal of 2,3,7,8-tetrachlorodibenzo-p-dioxin (TCDD) through the protein phosphorylation pathway. *Biochem Pharmacol* (1996) 52(10):1599–612. doi: 10.1016/S0006-2952(96)00566-7
15. Perdew GH. Association of the Ah receptor with the 90-kDa heat shock protein. *J Biol Chem* (1988) 263(27):13802–5. doi: 10.1016/S0021-9258(18)68314-0
16. Carver LA, Bradfield CA. Ligand-dependent interaction of the aryl hydrocarbon receptor with a novel immunophilin homolog *in vivo*. *J Biol Chem* (1997) 272(17):11452–6. doi: 10.1074/jbc.272.17.11452
17. Nair SC, Toran EJ, Rimerman RA, Hjermstad S, Smithgall TE, Smith DF. A pathway of multi-chaperone interactions common to diverse regulatory proteins: estrogen receptor, Fes tyrosine kinase, heat shock transcription factor Hsf1, and the aryl hydrocarbon receptor. *Cell Stress Chaperones* (1996) 1(4):237–50. doi: 10.1379/1466-1268(1996)001<0237:apomci>2.3.co;2
18. Reyes H, Reisz-Porszasz S, Hankinson O. Identification of the Ah receptor nuclear translocator protein (Arnt) as a component of the DNA binding form of the Ah receptor. *Science* (1992) 256(5060):1193–5. doi: 10.1126/science.256.5060.1193
19. Rothhammer V, Quintana FJ. The aryl hydrocarbon receptor: an environmental sensor integrating immune responses in health and disease. *Nat Rev Immunol* (2019) 19(3):184–97. doi: 10.1038/s41577-019-0125-8
20. Ohtake F, Baba A, Takada I, Okada M, Iwasaki K, Miki H, et al. Dioxin receptor is a ligand-dependent E3 ubiquitin ligase. *Nature* (2007) 446(7135):562–6. doi: 10.1038/nature05683
21. Luecke-Johansson S, Gralla M, Rundqvist H, Ho JC, Johnson RS, Gradin K, et al. A Molecular Mechanism To Switch the Aryl Hydrocarbon Receptor from a Transcription Factor to an E3 Ubiquitin Ligase. *Mol Cell Biol* (2017) 37(13):1–14. doi: 10.1128/MCB.00630-16
22. Jia Y, Tao Y, Lv C, Xia Y, Wei Z, Dai Y. Tetrandrine enhances the ubiquitination and degradation of Syk through an AhR-c-src-c-Cbl pathway and consequently inhibits osteoclastogenesis and bone destruction in arthritis. *Cell Death Dis* (2019) 10(2):38. doi: 10.1038/s41419-018-1286-2
23. Vogel CF, Sciuillo E, Li W, Wong P, Lazennec G, Matsumura F. RelB, a new partner of aryl hydrocarbon receptor-mediated transcription. *Mol Endocrinol* (2007) 21(12):2941–55. doi: 10.1210/me.2007-0211
24. Tian Y, Rabson AB, Gallo MA. Ah receptor and NF-kappaB interactions: mechanisms and physiological implications. *Chem Biol Interact* (2002) 141(1-2):97–115. doi: 10.1016/s0009-2797(02)00068-6
25. Domínguez-Acosta O, Vega L, Estrada-Muñiz E, Rodríguez MS, González FJ, Elizondo G. Activation of aryl hydrocarbon receptor regulates the LPS/IFN γ -induced inflammatory response by inducing ubiquitin-proteasomal and lysosomal degradation of RelA/p65. *Biochem Pharmacol* (2018) 155:141–9. doi: 10.1016/j.bcp.2018.06.016
26. Zhu J, Luo L, Tian L, Yin S, Ma X, Cheng S, et al. Aryl Hydrocarbon Receptor Promotes IL-10 Expression in Inflammatory Macrophages Through Src-STAT3 Signaling Pathway. *Front Immunol* (2018) 9:2033. doi: 10.3389/fimmu.2018.02033
27. Schubert K, Collins LE, Green P, Nagase H, Troeberg L. LRP1 Controls TNF Release via the TIMP-3/ADAM17 Axis in Endotoxin-Activated Macrophages. *J Immunol* (2019) 202(5):1501–9. doi: 10.4049/jimmunol.1800834
28. Schmidt JR, Geurtzen K, von Bergen M, Schubert K, Knopf F. Glucocorticoid Treatment Leads to Aberrant Ion and Macromolecular Transport in Regenerating Zebrafish Fins. *Front Endocrinol (Lausanne)* (2019) 10:674. doi: 10.3389/fendo.2019.00674
29. Hughes CS, Moggridge S, Muller T, Sorensen PH, Morin GB, Krijgsveld J. Single-pot, solid-phase-enhanced sample preparation for proteomics experiments. *Nat Protoc* (2019) 14(1):68–85. doi: 10.1038/s41596-018-0082-x
30. Wang Z, Karkossa I, Grosskopf H, Rolle-Kampczyk U, Hacker-muller J, von Bergen M, et al. Comparison of quantification methods in proteomics to define relevant toxicological information on AhR activation of HepG2 cells by BaP. *Toxicology* (2021) 448:152652. doi: 10.1016/j.tox.2020.152652
31. Cox J, Hein MY, Lubner CA, Paron I, Nagaraj N, Mann M. Accurate proteome-wide label-free quantification by delayed normalization and maximal peptide ratio extraction, termed MaxLFQ. *Mol Cell Proteomics* (2014) 13(9):2513–26. doi: 10.1074/mcp.M113.031591
32. UniProt C. UniProt: a worldwide hub of protein knowledge. *Nucleic Acids Res* (2019) 47(D1):D506–D15. doi: 10.1093/nar/gky1049
33. Ritchie ME, Phipson B, Wu D, Hu Y, Law CW, Shi W, et al. limma powers differential expression analyses for RNA-sequencing and microarray studies. *Nucleic Acids Res* (2015) 43(7):e47. doi: 10.1093/nar/gkv007
34. Wickham H. The Split-Apply-Combine Strategy for Data Analysis. *J Stat Softw* (2011) 40(1):1–29. doi: 10.18637/jss.v040.i01
35. Wickham H. Reshaping Data with reshapePackage. *J Stat Softw* (2007) 21(12):1–20. doi: 10.18637/jss.v021.i12
36. Dragulescu A, Arendt C. *xlsx: Read, Write, Format Excel 2007 and Excel 97/2000/XP/2003 Files. R package version 0.6.1.* (2018). Available at: <https://CRAN.R-project.org/package=xlsx>.
37. Zhang X, Smits AH, van Tilburg GB, Ovaa H, Huber W, Vermeulen M. Proteome-wide identification of ubiquitin interactions using UbIA-MS. *Nat Protoc* (2018) 13(3):530–50. doi: 10.1038/nprot.2017.147
38. Xiao N. *ggsci: Scientific Journal and Sci-Fi Themed Color Palettes for ggplot2. R package version 2.9.* (2018). Available at: <https://CRAN.R-project.org/package=ggsci>.
39. Gu Z, Gu L, Eils R, Schlesner M, Brors B. circlize implements and enhances circular visualization in R. *Bioinformatics* (2014) 30(19):2811–2. doi: 10.1093/bioinformatics/btu393
40. Graffelman J. *calibrate: Calibration of Scatterplot and Biplot Axes. R package version 1.7.5.* (2019). Available at: <https://CRAN.R-project.org/package=calibrate>.
41. Wickham H. *ggplot2: Elegant Graphics for Data Analysis.* Switzerland: Springer-Verlag New York (2016).
42. Wickham H, Bryan J. *readxl: Read Excel Files. R package version 1.3.1.* (2019). Available at: <https://CRAN.R-project.org/package=readxl>.

43. Spiess AN. *qpcR: Modelling and Analysis of Real-Time PCR Data. R package version 1.4-1.* (2018). Available at: <https://CRAN.R-project.org/package=qpcR>.
44. Mahto A. *splitstackshape: Stack and Reshape Datasets After Splitting Concatenated Values. R package version 1.4.8.* (2019). Available at: <https://CRAN.R-project.org/package=splitstackshape>.
45. Wickham H, Henry L. *tidyr: Tidy Messy Data. R package version 1.0.0.* (2019). Available at: <https://CRAN.R-project.org/package=tidyr>.
46. Turner S. *Tmisc: Turner Miscellaneous. R package version 0.1.22.* (2019). Available at: <https://CRAN.R-project.org/package=Tmisc>.
47. Bantscheff M, Schirle M, Sweetman G, Rick J, Kuster B. Quantitative mass spectrometry in proteomics: a critical review. *Anal Bioanal Chem* (2007) 389(4):1017–31. doi: 10.1007/s00216-007-1486-6
48. Pascovici D, Handler DC, Wu JX, Haynes PA. Multiple testing corrections in quantitative proteomics: A useful but blunt tool. *Proteomics* (2016) 16(18):2448–53. doi: 10.1002/pmic.201600044
49. Huang da W, Sherman BT, Lempicki RA. Systematic and integrative analysis of large gene lists using DAVID bioinformatics resources. *Nat Protoc* (2009) 4(1):44–57. doi: 10.1038/nprot.2008.211
50. Engholm-Keller K, Waardenberg AJ, Muller JA, Wark JR, Fernando RN, Arthur JW, et al. The temporal profile of activity-dependent presynaptic phospho-signalling reveals long-lasting patterns of poststimulus regulation. *PLoS Biol* (2019) 17(3):e3000170. doi: 10.1371/journal.pbio.3000170
51. Hornbeck PV, Zhang B, Murray B, Kornhauser JM, Latham V, Skrzypek E. PhosphoSitePlus, 2014: mutations, PTMs and recalibrations. *Nucleic Acids Res* (2015) 43(Database issue):D512–20. doi: 10.1093/nar/gku1267
52. Livak KJ, Schmittgen TD. Analysis of relative gene expression data using real-time quantitative PCR and the 2⁻(Delta Delta C(T)) Method. *Methods* (2001) 25(4):402–8. doi: 10.1006/meth.2001.1262
53. Ma Q, Baldwin KT. 2,3,7,8-Tetrachlorodibenzo-p-dioxin-induced Degradation of Aryl Hydrocarbon Receptor (AhR) by the Ubiquitin-Proteasome Pathway. *J Biol Chem* (2000) 275(12):8432–8. doi: 10.1074/jbc.275.12.8432
54. Davarinos NA, Pollenz RS. Aryl hydrocarbon receptor imported into the nucleus following ligand binding is rapidly degraded via the cytoplasmic proteasome following nuclear export. *J Biol Chem* (1999) 274(40):28708–15. doi: 10.1074/jbc.274.40.28708
55. Kalkhof S, Dautel F, Loguerco S, Baumann S, Trump S, Jungnickel H, et al. Pathway and time-resolved benzo[a]pyrene toxicity on Hepa1c1c7 cells at toxic and subtoxic exposure. *J Proteome Res* (2015) 14(1):164–82. doi: 10.1021/pr500957t
56. Boysen G, Hecht SS. Analysis of DNA and protein adducts of benzo[a]pyrene in human tissues using structure-specific methods. *Mutat Res* (2003) 543(1):17–30. doi: 10.1016/s1383-5742(02)00068-6
57. Pestell RG, Albanese C, Reutens AT, Segall JE, Lee RJ, Arnold A. The cyclins and cyclin-dependent kinase inhibitors in hormonal regulation of proliferation and differentiation. *Endocr Rev* (1999) 20(4):501–34. doi: 10.1210/edrv.20.4.0373
58. Arpa L, Valledor AF, Lloberas J, Celada A. IL-4 blocks M-CSF-dependent macrophage proliferation by inducing p21Waf1 in a STAT6-dependent way. *Eur J Immunol* (2009) 39(2):514–26. doi: 10.1002/eji.200838283
59. Das A, Yang CS, Arifuzzaman S, Kim S, Kim SY, Jung KH, et al. High-Resolution Mapping and Dynamics of the Transcriptome, Transcription Factors, and Transcription Co-Factor Networks in Classically and Alternatively Activated Macrophages. *Front Immunol* (2018) 9:22. doi: 10.3389/fimmu.2018.00022
60. Chow JC, Young DW, Golenbock DT, Christ WJ, Gusovsky F. Toll-like receptor-4 mediates lipopolysaccharide-induced signal transduction. *J Biol Chem* (1999) 274(16):10689–92. doi: 10.1074/jbc.274.16.10689
61. Lopez-Castejon G, Edelmann MJ. Deubiquitinases: Novel Therapeutic Targets in Immune Surveillance? *Mediators Inflammation* (2016) 2016:3481371. doi: 10.1155/2016/3481371
62. Cantrell DA. GTPases and T cell activation. *Immunol Rev* (2003) 192:122–30. doi: 10.1034/j.1600-065x.2003.00028.x
63. Yin Q, Jiang D, Li L, Yang Y, Wu P, Luo Y, et al. LPS Promotes Vascular Smooth Muscle Cells Proliferation Through the TLR4/Rac1/Akt Signalling Pathway. *Cell Physiol Biochem* (2017) 44(6):2189–200. doi: 10.1159/000486024
64. Sparfel L, Pinel-Marie ML, Boize M, Koscielny S, Desmots S, Pery A, et al. Transcriptional signature of human macrophages exposed to the environmental contaminant benzo(a)pyrene. *Toxicol Sci* (2010) 114(2):247–59. doi: 10.1093/toxsci/kfq007
65. Mimnaugh EG, Chen HY, Davie JR, Celis JE, Neckers L. Rapid deubiquitination of nucleosomal histones in human tumor cells caused by proteasome inhibitors and stress response inducers: effects on replication, transcription, translation, and the cellular stress response. *Biochemistry* (1997) 36(47):14418–29. doi: 10.1021/bi970998j
66. Udeshi ND, Mani DR, Eisenhaure T, Mertins P, Jaffe JD, Clauser KR, et al. Methods for quantification of *in vivo* changes in protein ubiquitination following proteasome and deubiquitinase inhibition. *Mol Cell Proteomics* (2012) 11(5):148–59. doi: 10.1074/mcp.M111.016857
67. Dantuma NP, Groothuis TA, Salomons FA, Neeffes J. A dynamic ubiquitin equilibrium couples proteasomal activity to chromatin remodeling. *J Cell Biol* (2006) 173(1):19–26. doi: 10.1083/jcb.200510071
68. Oughtred R, Stark C, Breitkreutz BJ, Rust J, Boucher L, Chang C, et al. The BioGRID interaction database: 2019 update. *Nucleic Acids Res* (2019) 47(D1):D529–D41. doi: 10.1093/nar/gky1079
69. Shao Y, Elly C, Liu YC. Negative regulation of Rap1 activation by the Cbl E3 ubiquitin ligase. *EMBO Rep* (2003) 4(4):425–31. doi: 10.1038/sj.embor.embor813
70. Dong B, Cheng W, Li W, Zheng J, Wu D, Matsumura F, et al. FRET analysis of protein tyrosine kinase c-Src activation mediated via aryl hydrocarbon receptor. *Biochim Biophys Acta (BBA) - Gen Subj* (2011) 1810(4):427–31. doi: 10.1016/j.bbagen.2010.11.007
71. Chung J, Serezani CH, Huang SK, Stern JN, Keskin DB, Jagirdar R, et al. Rap1 activation is required for Fc gamma receptor-dependent phagocytosis. *J Immunol* (2008) 181(8):5501–9. doi: 10.4049/jimmunol.181.8.5501
72. Li Y, Kim JG, Kim HJ, Moon MY, Lee JY, Kim J, et al. Small GTPases Rap1 and RhoA regulate superoxide formation by Rac1 GTPases activation during the phagocytosis of IgG-opsonized zymosans in macrophages. *Free Radic Biol Med* (2012) 52(9):1796–805. doi: 10.1016/j.freeradbiomed.2012.02.004
73. Visvikis O, Lores P, Boyer L, Chardin P, Lemichez E, Gacon G. Activated Rac1, but not the tumorigenic variant Rac1b, is ubiquitinated on Lys 147 through a JNK-regulated process. *FEBS J* (2008) 275(2):386–96. doi: 10.1111/j.1742-4658.2007.06209.x
74. Sanlioglu S, Williams CM, Samavati L, Butler NS, Wang G, McCray PB Jr, et al. Lipopolysaccharide induces Rac1-dependent reactive oxygen species formation and coordinates tumor necrosis factor-alpha secretion through IKK regulation of NF-kappa B. *J Biol Chem* (2001) 276(32):30188–98. doi: 10.1074/jbc.M102061200
75. Kanehisa M, Goto S. KEGG: kyoto encyclopedia of genes and genomes. *Nucleic Acids Res* (2000) 28(1):27–30. doi: 10.1093/nar/28.1.27
76. Gao Y, Dickerson JB, Guo F, Zheng J, Zheng Y. Rational design and characterization of a Rac GTPase-specific small molecule inhibitor. *Proc Natl Acad Sci USA* (2004) 101(20):7618–23. doi: 10.1073/pnas.0307512101
77. Gorzalczany Y, Sigal N, Itan M, Lotan O, Pick E. Targeting of Rac1 to the phagocyte membrane is sufficient for the induction of NADPH oxidase assembly. *J Biol Chem* (2000) 275(51):40073–81. doi: 10.1074/jbc.M006013200
78. Sarfstein R, Gorzalczany Y, Mizrahi A, Berdichevsky Y, Molshanski-Mor S, Weinbaum C, et al. Dual role of Rac in the assembly of NADPH oxidase, tethering to the membrane and activation of p67phox: a study based on mutagenesis of p67phox-Rac1 chimeras. *J Biol Chem* (2004) 279(16):16007–16. doi: 10.1074/jbc.M312394200
79. Linton MF, Moselehi JJ, Babaev VR. Akt Signaling in Macrophage Polarization, Survival, and Atherosclerosis. *Int J Mol Sci* (2019) 20(11):1–14. doi: 10.3390/ijms20112703
80. Vergadi E, Ieronymaki E, Lyroni K, Vaporidi K, Tsatsanis C. Akt Signaling Pathway in Macrophage Activation and M1/M2 Polarization. *J Immunol* (2017) 198(3):1006–14. doi: 10.4049/jimmunol.1601515
81. Brunet A, Bonni A, Zigmond MJ, Lin MZ, Juo P, Hu LS, et al. Akt promotes cell survival by phosphorylating and inhibiting a Forkhead transcription factor. *Cell* (1999) 96(6):857–68. doi: 10.1016/s0092-8674(00)80595-4
82. Lee JW, Nam H, Kim LE, Jeon Y, Min H, Ha S, et al. TLR4 (toll-like receptor 4) activation suppresses autophagy through inhibition of FOXO3 and impairs

- phagocytic capacity of microglia. *Autophagy* (2019) 15(5):753–70. doi: 10.1080/15548627.2018.1556946
83. Bouzeyen R, Haoues M, Barbouche MR, Singh R, Essafi M. FOXO3 Transcription Factor Regulates IL-10 Expression in Mycobacteria-Infected Macrophages, Tuning Their Polarization and the Subsequent Adaptive Immune Response. *Front Immunol* (2019) 10:2922. doi: 10.3389/fimmu.2019.02922
 84. Quintana FJ, Basso AS, Iglesias AH, Korn T, Farez MF, Bettelli E, et al. Control of T(reg) and T(H)17 cell differentiation by the aryl hydrocarbon receptor. *Nature* (2008) 453(7191):65–71. doi: 10.1038/nature06880
 85. Wheeler JL, Martin KC, Resseguie E, Lawrence BP. Differential consequences of two distinct AhR ligands on innate and adaptive immune responses to influenza A virus. *Toxicol Sci* (2014) 137(2):324–34. doi: 10.1093/toxsci/kft255
 86. Ehrlich AK, Pennington JM, Bisson WH, Kolluri SK, Kerkvliet NI. TCDD, FICZ, and Other High Affinity AhR Ligands Dose-Dependently Determine the Fate of CD4+ T Cell Differentiation. *Toxicol Sci* (2018) 161(2):310–20. doi: 10.1093/toxsci/kfx215
 87. Bohonowych JE, Denison MS. Persistent binding of ligands to the aryl hydrocarbon receptor. *Toxicol Sci* (2007) 98(1):99–109. doi: 10.1093/toxsci/kfm085
 88. Bergander L, Wincent E, Rannug A, Foroozesh M, Alworth W, Rannug U. Metabolic fate of the Ah receptor ligand 6-formylindolo[3,2-b]carbazole. *Chem Biol Interact* (2004) 149(2-3):151–64. doi: 10.1016/j.cbi.2004.08.005
 89. Wincent E, Amini N, Luecke S, Glatt H, Bergman J, Crescenzi C, et al. The suggested physiologic aryl hydrocarbon receptor activator and cytochrome P4501 substrate 6-formylindolo[3,2-b]carbazole is present in humans. *J Biol Chem* (2009) 284(5):2690–6. doi: 10.1074/jbc.M808321200
 90. Jin L, Li Y. Structural and functional insights into nuclear receptor signaling. *Adv Drug Delivery Rev* (2010) 62(13):1218–26. doi: 10.1016/j.addr.2010.08.007
 91. Denison MS, Soshilov AA, He G, DeGroot DE, Zhao B. Exactly the same but different: promiscuity and diversity in the molecular mechanisms of action of the aryl hydrocarbon (dioxin) receptor. *Toxicol Sci* (2011) 124(1):1–22. doi: 10.1093/toxsci/kfr218
 92. Zhao B, Degroot DE, Hayashi A, He G, Denison MS. CH223191 is a ligand-selective antagonist of the Ah (Dioxin) receptor. *Toxicol Sci* (2010) 117(2):393–403. doi: 10.1093/toxsci/kfq217
 93. Jin U-H, Lee S-O, Sridharan G, Lee K, Davidson LA, Jayaraman A, et al. Microbiome-Derived Tryptophan Metabolites and Their Aryl Hydrocarbon Receptor-Dependent Agonist and Antagonist Activities. *Mol Pharmacol* (2014) 85(5):777–88. doi: 10.1124/mol.113.091165
 94. Lamas B, Natividad JM, Sokol H. Aryl hydrocarbon receptor and intestinal immunity. *Mucosal Immunol* (2018) 11(4):1024–38. doi: 10.1038/s41385-018-0019-2
 95. Metidji A, Omenetti S, Crotta S, Li Y, Nye E, Ross E, et al. The Environmental Sensor AHR Protects from Inflammatory Damage by Maintaining Intestinal Stem Cell Homeostasis and Barrier Integrity. *Immunity* (2018) 49(2):353–62. doi: 10.1016/j.immuni.2018.07.010
 96. Deutsch EW, Bandeira N, Sharma V, Perez-Riverol Y, Carver JJ, Kundu DJ, et al. The ProteomeXchange consortium in 2020: enabling 'big data' approaches in proteomics. *Nucleic Acids Res* (2020) 48(D1):D1145–D52. doi: 10.1093/nar/gkz984

Conflict of Interest: The authors declare that the research was conducted in the absence of any commercial or financial relationships that could be construed as a potential conflict of interest.

Copyright © 2021 Großkopf, Walter, Karkossa, von Bergen and Schubert. This is an open-access article distributed under the terms of the Creative Commons Attribution License (CC BY). The use, distribution or reproduction in other forums is permitted, provided the original author(s) and the copyright owner(s) are credited and that the original publication in this journal is cited, in accordance with accepted academic practice. No use, distribution or reproduction is permitted which does not comply with these terms.